



Chemical characterization of oxygenated organic compounds in the gas phase and particle phase using iodide CIMS with FIGAERO in urban air

Chenshuo Ye¹, Bin Yuan^{2,3}, Yi Lin^{2,3}, Zelong Wang^{2,3}, Weiwei Hu⁴, Tiange Li^{2,3}, Wei Chen⁴, Caihong Wu^{2,3}, Chaomin Wang^{2,3}, Shan Huang^{2,3}, Jipeng Qi^{2,3}, Baolin Wang⁵, Chen Wang⁵, Wei Song⁴, Xinming Wang⁴, E Zheng^{2,3}, Jordan E. Krechmer⁶, Penglin Ye⁷, Zhanyi Zhang^{2,3}, Xuemei Wang^{2,3}, Douglas R. Worsnop⁶, and Min Shao^{2,3,1}

¹College of Environmental Sciences and Engineering, Peking University, Beijing 100871, China

²Institute for Environmental and Climate Research, Jinan University, Guangzhou 511443, China

³Guangdong–Hong Kong–Macau Joint Laboratory of Collaborative Innovation for Environmental Quality, Guangzhou 511443, China

⁴Guangzhou Institute of Geochemistry, Chinese Academy of Sciences, Guangzhou 511443, China

⁵School of Environmental Science and Engineering, Qilu University of Technology, Jinan 250353, China

⁶Aerodyne Research, Inc., 45 Manning Rd., Billerica, MA, USA

⁷Shanghai Key Laboratory of Atmospheric Particle Pollution and Prevention (LAP³), Department of Environmental Science and Engineering, Fudan University, Shanghai 200438, China

Correspondence: Bin Yuan (byuan@jnu.edu.cn)

Received: 14 November 2020 – Discussion started: 25 November 2020

Revised: 16 April 2021 – Accepted: 24 April 2021 – Published: 3 June 2021

Abstract. The atmospheric processes under polluted environments involving interactions of anthropogenic pollutants and natural emissions lead to the formation of various and complex secondary products. Therefore, the characterization of oxygenated organic compounds in urban areas remains a pivotal issue in our understanding of the evolution of organic carbon. Here, we describe measurements of an iodide chemical ionization time-of-flight mass spectrometer installed with a Filter Inlet for Gases and AEROsols (FIGAERO-I-CIMS) in both the gas phase and the particle phase at an urban site in Guangzhou, a typical megacity in southern China, during the autumn of 2018. Abundant oxygenated organic compounds containing two to five oxygen atoms were observed, including organic acids, multi-functional organic compounds typically emitted from biomass burning, oxidation products of biogenic hydrocarbons and aromatics. Photochemistry played dominant roles in the formation of gaseous organic acids and isoprene-derived organic nitrates, while nighttime chemistry contributed significantly to the formation of monoterpene-derived organic nitrates and inorganics. Nitrogen-containing organic compounds occupied a significant fraction of the total signal in both the gas and particle

phases, with elevated fractions at higher molecular weights. Measurements of organic compounds in the particle phase by FIGAERO-I-CIMS explained $24 \pm 0.8\%$ of the total organic aerosol mass measured by aerosol mass spectrometer (AMS), and the fraction increased for more aged organic aerosol. The systematical interpretation of mass spectra of the FIGAERO-I-CIMS in the urban area of Guangzhou provides a holistic view of numerous oxygenated organic compounds in the urban atmosphere, which can serve as a reference for the future field measurements by FIGAERO-I-CIMS in polluted urban regions.

1 Introduction

In urban air, atmospheric chemical processes are varied and complex, as the result of large emissions of both anthropogenic pollutants and biogenic volatile organic compounds, associated with strong interactions with each other (He et al., 2014; Karl et al., 2018; Shrivastava et al., 2019). Consequently, strong formation of secondary pollutants, e.g., ozone

and secondary organic aerosol (SOA), are observed in urban and downwind regions (Huang et al., 2015; Zhang et al., 2014). Oxygenated organic compounds are not fully accounted for in some earlier studies, which may explain some of the discrepancies between observations and models for many unaddressed issues in atmospheric chemistry. Oxygenated organic compounds are supposed to be the top candidates for missing OH reactivity observed in various environments including pristine rainforests and urbanized areas (Noelscher et al., 2016; Yang et al., 2016, 2017). The photolysis of carbonyls serves as a critical radical source driving ozone formation in highly polluted industrialized areas (Edwards et al., 2014; Liu et al., 2012; Xue et al., 2016). Although it was discovered a long time ago that oxygenated organic compounds make up a substantial fraction of submicron aerosol mass (Kroll and Seinfeld, 2008), enormous difficulty still exists in accurately predicting the formation and evolution of SOA (de Gouw et al., 2005; Hodzic et al., 2010; Volkamer et al., 2006).

One of the biggest obstacles to understanding the role of oxygenated organic compounds is the characterization of these extremely complicated and diverse chemicals which encompass tens of thousands of individual species spanning a wide range of volatility. Chemical ionization mass spectrometry (CIMS) is a powerful technique for the molecular-level characterization of oxygenated organic compounds because of the following advantages (Zhao, 2018): direct measurements and fast time response to capture the rapid temporal change of short-lifetime intermediates, soft ionization providing chemical information on a molecular level, and selective ionization ensuring measurements for specific classes of species. The iodide anion ionizes species mainly through adduction (Iyer et al., 2016) and is used for the detection of oxygenated organic compounds, particularly organic compounds with two to five oxygen atoms (Lee et al., 2014; Lopez-Hilfiker et al., 2016; Riva et al., 2019). It has been shown that I-CIMS is an excellent technique to investigate the oxidation processes of volatile organic compounds (VOCs) and formation of SOA (Isaacman-VanWertz et al., 2018). Installed with a thermal desorption inlet that collects and heats aerosol to evaporate organic compounds, e.g., Filter Inlet for Gases and AEROSols (FIGAERO, Lopez-Hilfiker et al., 2014) and Micro-Orifice Volatilization Impactor (MOVI, Yatavelli et al., 2012), the CIMS instruments are capable of analyzing particle-phase species and gas-particle partitioning in a semi-continuous way (Stark et al., 2017; Stolzenburg et al., 2018).

Although FIGAERO-CIMS has gained recent popularity in atmospheric chemistry research, much of the published work was done in chambers or in the laboratory (D'Ambro et al., 2017, 2018; Hammes et al., 2019; Lopez-Hilfiker et al., 2015). As for the applications in field campaigns, most work has been mostly performed in forest or rural areas (Huang et al., 2019; Hunter et al., 2017; Lee et al., 2016, 2018b); measurements in the urban atmosphere by FIGAERO-CIMS are still limited (Le Breton et al., 2018b). Meanwhile, a sys-

tematic analysis on mass spectra of FIGAERO-CIMS in the ambient air is imperative, for a more holistic view in investigating emissions and chemistry of oxygenated organic compounds. In this study, we present the measurement results using FIGAERO-I-CIMS during a coordinated campaign in Guangzhou, a megacity in the Pearl River region of China. We describe the experimental design, instrumentation setup, calibration and data processing for this instrument in the campaign. This work will provide a detailed interpretation of the mass spectra of oxygenated species in both the gas phase and the particle phase. The bulk chemical properties will also be discussed to provide an overview of organic compounds.

2 Methods

2.1 Measurement site and supporting data

Measurements were conducted during the coordinated campaign “Particles, Radicals and Intermediates from oxidation of primary Emissions over the Great Bay Area” (PRIDE-GBA) in October and November 2018. The Great Bay Area (GBA) refers to a highly industrialized and urbanized area in southern China, including the two special administrative regions of Hong Kong and Macau, and nine cities surrounding the Pearl River estuary. Affected by the subtropical monsoon climate, the weather in the region was characterized by high temperatures and relative humidity (RH) as well as sufficient sunshine (total solar radiation of the Pearl River Delta region in the fall of 2016 was $\sim 1200 \text{ MJ/m}^2$, Liu et al., 2018). The city of Guangzhou lies in the north of the GBA and south of the mountains. Therefore, the city is extensively influenced by both anthropogenic and biogenic emissions. The urban site was located at Guangzhou Institute of Geochemistry, Chinese Academy of Sciences (23.14° N , 113.36° E). Online instruments sampled from inlets set up in laboratories on the eighth floor or ninth floor (about 25 m above the ground).

In addition to FIGAERO-I-CIMS discussed later, measurement data from a suite of other instruments were also used in this work. A high-resolution time-of-flight aerosol mass spectrometer (HR-ToF-AMS, Aerodyne Research, Inc.) was deployed to provide chemical composition and many other parameters of ambient aerosol including f_{60} , liquid water content (LWC), particulate organic nitrate and elemental ratios (Hu et al., 2016, 2018). The parameter f_{60} is the ratio of the integrated signal at m/z 60 to the total signal of organic components and is used as a tracer for biomass burning emissions (Cubison et al., 2011). LWC of aerosol was taken as the sum of water contributed by inorganic components predicted by the ISORROPIA II model and organic components calculated based on the organic hygroscopicity parameter (Fountoukis and Nenes, 2007; Guo et al., 2015). Based on AMS data, organic nitrate concentrations were determined by 2–3 times lower $\text{NO}_2^+ / \text{NO}^+$ ratios

for organic nitrate than inorganic nitrate (Fry et al., 2013). The calculation method of elemental ratios based on AMS data has been described elsewhere (Aiken et al., 2007; Canagaratna et al., 2015). Detailed information about AMS measurements from the PRIDE-GBA campaign is forthcoming in a separate paper. An online GC-MS/FID (Wuhan Tianhong Instrument Co., Ltd) and a proton transfer reaction time-of-flight mass spectrometer (PTR-ToF-MS, IONICON Analytik GmbH) (Yuan et al., 2017) served as the analytical techniques for measuring isoprene and other VOCs (e.g., monoterpenes, aromatics and a few oxygenated VOCs) (Wu et al., 2020), respectively. Trace gases (CO, O₃, NO and NO₂) were measured by commercial gas monitors (Thermo Fisher Scientific Inc.) (Z. Wang et al., 2020). Photolysis rates were measured by a PFS-100 photolysis spectrometer (Focused Photonics Inc.). Temperature and RH were measured by a Vantage Pro2 weather station (Davis Instruments Corp.). Time series and diurnal profiles of meteorological parameters, trace gases, the photolysis rate of NO₂ (J_{NO_2}) and several important VOCs (isoprene, monoterpenes, toluene and benzene) are shown in Fig. S1. The temperature during the campaign was between 17 and 33 °C, with an average of 24 °C, and RH was between 27 % and 97 %, with an average of 70 %.

2.2 FIGAERO-I-CIMS

2.2.1 Experimental setup

Our instrument consists of a Filter Inlet for Gases and AEROSols (FIGAERO) and a time-of-flight chemical ionization mass spectrometer coupled with an iodide ionization source (Bertram et al., 2011; Lee et al., 2014; Lopez-Hilfiker et al., 2014). The FIGAERO is a multi-port inlet assembly following a two-step procedure alternating between gas mode, in which online measurements of gases and semi-continuous sampling of particle-phase species are conducted, and particle mode, in which particulate composition is investigated via thermal desorption (Lopez-Hilfiker et al., 2014; Thornton et al., 2020). The iodide source is a “soft” ionization technique with little ionization-induced fragmentation and selective detection towards multi-functional organic compounds, providing elemental compositions for thousands of oxygenated compounds in the atmosphere (Hyytinen et al., 2018; Iyer et al., 2016; Lee et al., 2014; Riva et al., 2019).

The sample air was drawn into the ion molecule reaction (IMR) chamber where it intersected and reacted with primary ions generated by flowing 2 mL/min 1000 ppm methyl iodide in 2.4 L/min N₂ through an X-ray source. The pressure in the IMR chamber was maintained at 370–390 mbar. Equipped with a long time-of-flight mass analyzer, our instrument was configured to measure singularly charged ions up to 603 Th with a mass resolving power of 10 000–11 000 ($m/\Delta m$ at 50 % height) during the campaign (Fig. S2).

Ambient air was continuously sampled through two inlets protruding about 1.5 m out of a window on the ninth floor of a building. One was a 3 m PFA tubing (1/4 in. o.d.) for gas-phase sampling, through which roughly 9 L/min air was drawn, and 2 L/min was directly taken into the instrument for gas measurements without removing particles, resulting in an inlet residence time of 0.24 s. The gas sampling line inside the room was covered by heat insulation associated with a heating cable to minimize condensation on the tubing surface. The other inlet for the particle phase was a 3.8 m metal tubing (3/8 in. o.d.) fitted with a PM_{2.5} cyclone and a Nafion dryer (Perma Pure, model PD-07018T-12MSS) to reduce water content in the sampled air. The particle-phase inlet was drawn by a laminar flow at ~ 8 L/min (Reynolds number of ~ 1500), 3.8 L/min of which was collected on PTFE membrane filters (Zefluor®, Pall Inc., USA). The residence time was 1.3 s for the particle-phase sampling line. Semi-volatility and low-volatility compounds tend to interact with wall surfaces of both inlets and the IMR and thus extend response time (Krechmer et al., 2016). As accurate correction for wall losses remains impossible, no wall loss correction was performed in this study.

The FIGAERO worked in a cyclical 1 h pattern with two modes (Fig. S3): (i) measuring gas for the first 24 min while simultaneously collecting particles on the filter and (ii) then analyzing the particle-phase collection for another 36 min. In every 24 min gas mode, ambient air was measured for the first 21 min, followed by 3 min gas background by over-flowing zero air at 5 L/min through a pinhole just in front of the IMR. The background measurements are inevitably influenced by wall interactions, especially for “sticky” species. Recently, Palm et al. (2019) proposed a new way to determine gas background (“fast background”) by fast switching between the ambient air and background, which greatly improves accurate determination of the CIMS background. In the remaining 36 min, the components of the collected particles were thermally desorbed and introduced into the CIMS with 2 L/min N₂ carrier gas. The N₂ flow was ramped from ambient temperature to 175 °C in 12 min and held for another 20 min. A schematic diagram of working modes and temperature profile of FIGAERO heating in a single cycle are shown in Fig. S4. Particle background was determined every sixth 1 h running cycle in which ambient air passed over a filter (Parker Balston, model 9922-11-CQ) in front of the FIGAERO filter.

2.2.2 Calibration experiments

Using various techniques, we calibrated dozens of chemical compounds in the laboratory. Table S1 summarizes the calibrated species and corresponding calibration methods. (1) Gas cylinders are commercially available for a few species (e.g., chlorine, hydrogen cyanide). The gaseous standards were diluted down to different concentrations and then introduced to the CIMS. (2) For those VOCs whose stan-

dards are liquid or solid, solutions with known concentrations are made and then vaporized using the liquid calibration unit (LCU, IONICON Analytik GmbH) to provide gaseous standards. (3) Commercial permeation tubes are available for some species (e.g., nitric acid). (4) Some gaseous chemicals were generated in the laboratory. For example, isocyanic acid was generated from thermal decomposition of cyanuric acid in a diffusion cell (Li et al., 2021; Z. Wang et al., 2020), and dinitrogen pentoxide was generated via the reaction of ozone with excess nitrogen dioxide in a flow reactor (Bertram et al., 2009). (5) Compounds of low vapor pressure were calibrated through the FIGAERO (Lopez-Hilfiker et al., 2014). Briefly, certain amounts of target species dissolved in organic solvents (e.g., isopropanol or acetone) were deposited onto the PTFE filter of the FIGAERO using a syringe, and the droplet was then subjected to a temperature-programmed thermal desorption by N_2 gas. The sensitivity was determined as the integrated signals under thermogram profiles versus the amounts of deposited calibrant.

In addition to sensitivity calibration, the effect of humidity on the sensitivity for various species was investigated in the laboratory, some of which are shown in Fig. S5. Low-molecular-weight acids, e.g., formic acid and nitric acid, tend to be more sensitive to the humidity changes than multi-functional compounds. A similar tendency of multi-functional compounds associated with less humidity dependence was also reported in previous work (Lee et al., 2014). Considering water vapor pressure in the IMR, our humidity-dependent curves are generally consistent with those reported in Lee et al. (2014) (see detailed discussions in Sect. S3 in the Supplement).

In the later part of the campaign (after 22 October), an isotopically labeled formic acid (DCOOH, Cambridge Isotope Laboratories, Inc.) permeation tube held at constant temperature (65°) was mixed with 10 mL/min N_2 and continuously delivered into the entrance of the sampling inlet in order to derive a humidity dependence function from the field measurements. DCOOH signals during the campaign exhibited a humidity-dependent curve consistent with formic acid obtained in the laboratory (Fig. S5). We applied humidity correction to the species with the humidity-dependent curves determined in the laboratory (underlined species in Table S1). For other compounds, humidity correction was not applied, as there is no universal pattern of humidity dependence for all detected species, and multi-functional compounds that comprise the majority of the species measured by FIGAERO-I-CIMS are usually less influenced by humidity.

The measured concentration of DCOOH was steady after humidity correction was applied (Fig. S6g), indicating the stability of our instrument. In addition, we also performed field calibrations throughout the campaign to check the instrument status by spotting a solution mixture of levoglucosan, heptaethylene glycol and octaethylene glycol onto the FIGAERO filter every 2–3 d (Fig. S6). Multiple-point calibrations for these organic species were performed in the be-

ginning and the end of the campaign. The concentration of the solution used in the first two calibration experiments was too high, so we prepared a new solution for calibrations in November. The relative changes of the determined calibration factors in November were within 50 % for the calibrated species.

2.2.3 Data processing

The TofWare software (version 3.0.3; Tofwerk AG, Switzerland) was used to conduct the high-resolution peak fitting for the mass spectra data of ToF-CIMS, including mass calibration, instrumental parameter optimization (peak shape and peak width) and bunch fitting of high-resolution peaks (Stark et al., 2015). In this study, the signals of ions were normalized to the sum signals of I^- and H_2OI^- at 10^6 cps. Hourly particle-phase data were obtained by integrating the signals of various ions during each FIGAERO desorption period. Background-corrected signals were obtained by subtracting linearly interpolated background signals from ambient signals (and integrated signals) for ions in the gas (and particle) phase.

In order to determine the sensitivities of uncalibrated species, a voltage scanning procedure was performed from time to time throughout the campaign covering different times of the day (Iyer et al., 2016; Lopez-Hilfiker et al., 2016). Here, we selected four representative periods including morning, afternoon, evening and night on polluted days. By performing sigmoidal fitting on the remaining signals as a function of voltages, a dV_{50} value of each ion from each period was determined, at which voltage half of one kind of ion dissociated (Lopez-Hilfiker et al., 2016). We observed a positive correlation between the sensitivities of the ions relative to maximum sensitivity and their average dV_{50} values (Fig. S7), consistent with previous studies (Isaacman-VanWertz et al., 2018; Lopez-Hilfiker et al., 2016). This relationship was used to calculate response factors for uncalibrated species, after taking into account the relative transmission efficiency for the ions (see Sect. S1 in the Supplement for detailed analysis).

3 Results and discussion

3.1 Overview of detected species in the mass spectra

We identify 1334 ions adducted with iodide from the mass spectra, among which 427 are charged closed-shell organic compounds containing only C, H and O elements ($C_xH_yO_zI^-$) and 388 are charged closed-shell organic compounds containing C, H, O and N elements ($C_xH_yN_{1,2}O_zI^-$). For species with the formula of $C_xH_yO_z$, x ranges from 1 to 20, y is an even number and no more than $2x + 2$, and z is greater than or equal to 2. The range of carbon number x for the ions with $C_xH_yN_{1,2}O_z$ is the same as the ions with $C_xH_yO_z$. For species containing one nitrogen ($C_xH_yNO_z$),

y is an odd number and less than $2x + 2$; z is larger than or equal to 2. For species containing two nitrogen atoms ($C_xH_yN_2O_z$), y is an even number and less than $2x + 1$; z is larger than or equal to 4. Table 1 summarizes species discussed in the main text. Although iodide clusters with two nitrogen atoms and zero nitrogen atoms both lie on odd masses, they can be separated for certain ions with the current resolving power, as demonstrated by the peak fitting results of mass spectrum at m/z 311 (Fig. S8).

The campaign-averaged mass spectra of detected ions in the both gas and particle phases are shown in Fig. 1. In general, molecules in the particle phase have larger molecular weights compared to those in the gas phase. Signals in the mass range of 150–300 Th comprise a large fraction of gas-phase compounds, and concentrations in the gas phase decrease quickly with m/z higher than 250 Th. In contrast, the detected signals in the particle phase are mainly distributed within the range of 200–320 Th.

Average nighttime (22:00–06:00) and daytime (10:00–18:00) mixing ratios for various species were shown in Fig. 2. Most species have higher concentrations during the daytime, especially for relatively volatile compounds in the gas phase, despite the fact that lower boundary layer height at night should increase nighttime concentration, as many primary gases behaved, e.g., CO (Fig. S1) (Wu et al., 2020). The higher concentrations during the daytime for most species detected by FIGAERO-I-CIMS suggest the dominant role of photochemical-induced oxidation in forming these oxidized compounds. In addition to typical nocturnal species including nitryl chloride ($ClNO_2I^-$), chlorine nitrate ($ClONO_2I^-$) and dinitrogen pentoxide ($N_2O_5I^-$), higher concentrations for the ions of $C_6H_{10}O_5I^-$ and $C_6H_{12}O_5I^-$ were also observed, which will be discussed in the next section. A large number of particulate N-containing organic compounds increase at night as well, as shown by mass defect diagrams of $C_xH_yO_z$ and $C_xH_yN_{1,2}O_z$ color-coded by the night-to-day ratios (Fig. S9).

Based on the mass spectra shown in Fig. 1, we identify a number of ions associated with high concentrations in both the gas phase and the particle phase. In the following Sect. 3.2–3.7, we will perform interpretation of the mass spectra by analyzing variability and correlation of these important ions, including monosaccharide-derived compounds (with brown tags in Fig. 1), oxygenated aromatics (with purple tags), organic acids (with pink tags), oxidation products of biogenic volatile organic compounds (BVOCs, with green tags), sulfur-containing compounds and inorganics (with blue tags). After going through detailed analysis at the species level, Sect. 3.8 will provide an overall picture about bulk chemical characteristics of detected organic compounds in terms of the distributions of average carbon oxidation states, carbon number and oxygen number. Lastly, Sect. 3.9 will compare our measurement of organic aerosol (OA) with AMS data.

3.2 Monosaccharide-derived compounds

$C_6H_{10}O_5$ and $C_6H_{12}O_5$ are highly correlated with each other in aerosol ($r = 0.92$), and they are two of the few $C_xH_yO_z$ compounds with higher concentrations at night. Previous work attributed them to monosaccharide-derived compounds emitted from biomass burning (Bhattacharai et al., 2019; Qi et al., 2019; Reyes-Villegas et al., 2018; Simoneit et al., 1999).

In this campaign, $C_6H_{10}O_5$ was detected mostly in the particle phase (the fraction in the particle phase $F_p = 0.81 \pm 0.09$) with an average concentration of $0.073 \pm 0.076 \mu\text{g}/\text{m}^3$. Its diurnal profile started increasing at dusk, reaching a peak at about midnight, and then fell off, as shown in Fig. 3. The mass fraction of $C_6H_{10}O_5$ in OA had a similar diurnal profile, and the ratios of $C_6H_{10}O_5$ to CO increased at night (from 0.17 ± 0.02 to $0.5 \pm 0.03 \mu\text{g m}^{-3}/\text{ppm}$, Fig. 3c), both suggesting enhanced emissions of this compound were related with combustion activities in the evening, e.g., residential biofuel burning for cooking as reported by some previous measurements in China (Q. Wang et al., 2020; Zhang et al., 2015). Furthermore, the time variations of particle-phase $C_6H_{10}O_5I^-$ were very similar to those of the m/z 60 fragment in AMS mass spectra (Fig. 3a), which is an identified tracer of biomass burning OA produced from the thermal decomposition of levoglucosan and similar compounds on the vaporizer of AMS (Brege et al., 2018; Cubison et al., 2011; Schneider et al., 2006). Therefore, $C_6H_{10}O_5$ was probably levoglucosan and its isomers (mannosan and galactosan), and $C_6H_{12}O_5$ was probably also a monosaccharide compound that had sources similar to $C_6H_{10}O_5$.

3.3 Oxygenated aromatic compounds

Combustion activities emit a great deal of compounds besides saccharides that the I-CIMS instrument can detect, including nitro-aromatics and guaiacol derivatives (Gaston et al., 2016; Kong et al., 2021). Nitro-benzenediols ($C_6H_5NO_4I^-$) as well as the highly correlated homologue methyl nitro-benzenediols ($C_7H_7NO_4I^-$) ($r = 0.88$ in the particle phase) exhibited double peaks in their diurnal profiles (Fig. 4). One was in the evening, similar to levoglucosan ($C_6H_{10}O_5$). The other peak was at noon. The scatterplot of $C_6H_5NO_4$ as the function of $C_6H_{10}O_5$ exhibits two different slopes (Fig. 5): the lower slope at night (0.088 ± 0.005) indicates the contribution of biomass burning, while the higher slope during the daytime (0.26 ± 0.02) suggests there were other important sources for nitro-aromatics, potentially secondary formation from photooxidation of aromatics (Jenkin et al., 2003). Guaiacol derivatives may have similar sources with nitro-aromatics, as implied by the resemblance of the scatterplots of these two chemical classes versus levoglucosan (cf., Figs. S10 and 5).

Nitrophenols ($C_6H_5NO_3I^-$), methyl nitrophenols ($C_7H_7NO_3I^-$) and dinitrophenols ($C_6H_4N_2O_5I^-$) were the

Table 1. The detected ions discussed in the text.

Ion formula	<i>m/z</i>	Attributed compounds	Possible formation pathways	References
C ₆ H ₁₀ O ₅ I ⁻	288.96	Levoglucosan, mannosan and galactosan	Biomass burning or cooking emissions	Gaston et al. (2016); Reyes-Villegas et al. (2018)
C ₆ H ₁₂ O ₅ I ⁻	290.97	Fucose	Biomass burning emissions	Qi et al. (2019)
C ₆ H ₅ NO ₃ I ⁻	265.93	Nitro-phenols	Direct emissions, oxidation of aromatics in the presence of NO _x	Gaston et al. (2016); Yuan et al. (2016)
C ₆ H ₅ NO ₄ I ⁻	281.93	Nitro-benzenediols	Direct emissions, oxidation of aromatics in the presence of NO _x	Gaston et al. (2016); Yuan et al. (2016)
C ₆ H ₄ N ₂ O ₅ I ⁻	310.92	Dinitro-phenols	Direct emissions, oxidation of aromatics in the presence of NO _x	Gaston et al. (2016); Yuan et al. (2016)
C ₇ H ₇ NO ₃ I ⁻	279.95	Methyl nitro-phenols	Direct emissions, oxidation of aromatics in the presence of NO _x	Gaston et al., 2016; Yuan et al., 2016)
C ₇ H ₇ NO ₄ I ⁻	295.94	Methyl nitro-benzenediols	Direct emissions, oxidation of aromatics in the presence of NO _x	Gaston et al. (2016); Yuan et al. (2016)
C ₇ H ₆ O ₄ I ⁻	280.93	Dihydroxy methyl benzoquinone	Aromatics + OH	Schwantes et al. (2017); M. Wang et al. (2020)
C ₇ H ₈ O ₄ I ⁻	282.95	Tetrahydroxy toluene	Aromatics + OH	Schwantes et al. (2017); M. Wang et al. (2020)
C ₇ H ₈ O ₅ I ⁻	298.94	Pentahydroxy toluene, fragments of C ₉ aromatics	Aromatics + OH	Mehra et al. (2020); Schwantes et al. (2017)
CH ₂ O ₂ I ⁻	172.91	Formic acid	Oxidation of VOCs	Lee et al. (2014); Yuan et al. (2015)
C ₂ H ₄ O ₂ I ⁻	186.93	Acetic acid	Oxidation of VOCs	Lee et al. (2014); Mattila et al. (2018)
C ₅ H ₁₀ O ₂ I ⁻	228.97	Pentanoic acid	Traffic emissions, secondary formation	Mattila et al. (2018)
C ₂ H ₄ O ₃ I ⁻	202.92	Glycolic acid	Oxidation of VOCs	Lee et al. (2014); Lim et al. (2005)
C ₃ H ₄ O ₃ I ⁻	214.92	Pyruvic acid	Photolysis of methylglyoxal, BVOCs + OH, photooxidation of aromatics in the presence of NO _x	Eger et al. (2020); Mattila et al. (2018)
C ₂ H ₂ O ₄ I ⁻	216.90	Oxalic acid	Aqueous-phase photooxidation of glyoxal, photooxidation of VOCs	Carlton et al. (2007); Lee et al. (2014); Zhou et al. (2015)
C ₃ H ₄ O ₄ I ⁻	230.92	Malonic acid, hydroxypyruvic acid	Oxidation of VOCs	Kawamura and Bikkina (2016); Lee et al. (2014)
C ₄ H ₄ O ₄ I ⁻	242.92	Maleic acid, fumaric acid	Oxidation of aromatics	Brege et al. (2018); Kawamura et al. (1996)
C ₅ H ₆ O ₄ I ⁻	256.93	Unsaturated dicarboxylic acid	Oxidation of aromatics	Brege et al. (2018); Kawamura et al. (1996)
C ₅ H ₈ O ₄ I ⁻	258.95		Photooxidation of VOCs	Berndt et al. (2019); Kawamura and Bikkina (2016)
C ₆ H ₁₀ O ₄ I ⁻	272.96		Photooxidation of VOCs	Berndt et al. (2019); Kawamura and Bikkina (2016)
C ₄ H ₈ O ₄ I ⁻	246.95	2-methylglyceric acid	Isoprene SOA component under high-NO _x conditions	Surratt et al. (2006, 2010)

Table 1. Continued.

Ion formula	<i>m/z</i>	Attributed compounds	Possible formation pathways	References
C ₅ H ₉ NO ₄ I ⁻	273.96	IHN (isoprene hydroxy nitrates)	First-generation organic nitrates from reaction: isoprene + OH + NO _x , isoprene + NO ₃	Jacobs et al. (2014); Xiong et al. (2015)
C ₄ H ₇ NO ₅ I ⁻	275.94	MVKN/ MACRN	Second-generation organic nitrates from oxidation of IHN in the presence of NO _x	Fisher et al. (2016); Paulot et al. (2009)
C ₅ H ₉ NO ₅ I ⁻	289.95	C ₅ nitrooxy hydroperoxide, C ₅ nitrooxy hydroxyepoxide, C ₅ dihydroxy nitrate	isoprene + NO ₃ , isoprene + OH + NO _x	iso- Ng et al. (2017); Schwantes et al. (2015); Wennberg et al. (2018)
C ₈ H ₁₂ O ₄ I ⁻	298.98	Dicarboxylic and oxocarboxylic acids like norpinic acid, terpenylic acid	Monoterpenes + OH, monoterpenes O ₃	Fang et al. (2017); Mutzel et al. (2016); Yasmeeen et al. (2011)
C ₉ H ₁₄ O ₄ I ⁻	312.99	Dicarboxylic and oxocarboxylic acids like pinic acid, homoterpenylic acid, caric acid	Monoterpenes + OH, monoterpenes O ₃	Fang et al. (2017); Mutzel et al. (2016); Yasmeeen et al. (2011)
C ₁₀ H ₁₆ O ₃ I ⁻	311.02	Oxocarboxylic acids like pinonic acid, caronic acid	Monoterpenes + OH, monoterpenes O ₃	Fang et al. (2017); Glasius et al. (2000); Yasmeeen et al. (2011)
C ₈ H ₁₃ NO ₆ I ⁻	345.98	Organic nitrates from monoterpenes	Monoterpenes + OH + NO _x , monoterpenes + NO ₃	Lee et al. (2016); Nah et al. (2016)
C ₈ H ₁₁ NO ₇ I ⁻	359.96	Organic nitrates from monoterpenes	Monoterpenes + OH + NO _x , monoterpenes O ₃ + NO ₃	Carlsaw (2013); Lee et al. (2016)
C ₁₀ H ₁₅ NO ₆ I ⁻	372.00	Organic nitrates from monoterpenes, peroxyacetyl nitrate from pinonaldehyde	Monoterpenes + OH + NO _x , monoterpenes O ₃ + NO ₃	Boyd et al. (2015); Massoli et al. (2018); Schwantes et al. (2020)
HSO ₄ ⁻	96.96	Sulfuric acid	Oxidation of SO ₂	Le Breton et al. (2018b)
SO ₃ I ⁻	206.86	Sulfur trioxide, fragment of organosulfates	Oxidation of SO ₂ , decomposition of organosulfates	Surratt et al. (2007)
C ₂ H ₃ SO ₆ ⁻	154.96	Glycolic acid sulfate	Aqueous reaction of glycolic acid and sulfuric acid	Galloway et al. (2009); Huang et al. (2018)
CH ₃ SO ₃ ⁻	94.98	Methanesulfonic acid	Oxidation of dimethyl sulfide	Chen and Finlayson-Pitts (2017); Gondwe et al. (2003)
N ₂ O ₅ I ⁻	234.89	Dinitrogen pentoxide	NO ₃ + NO ₂ + M	Le Breton et al. (2018a); Wang et al. (2016)
ClNO ₂ I ⁻	207.87	Nitryl chloride	N ₂ O ₅ (g) + Cl ⁻ (aq)	Le Breton et al. (2018a); Wang et al. (2016)
ClNO ₃ I ⁻	223.86	Chlorine nitrate	ClO + NO ₂ + M	Liu et al. (2017); Sander and Crutzen (1996)
Cl ₂ I ⁻	196.84	Chlorine	Heterogeneous reactions of Cl ⁻ and reactive chlorine like HOCl and ClNO ₂	Le Breton et al. (2018a); Liu et al. (2017); Wang et al. (2019)
HNO ₃ I ⁻	189.90	Nitric acid	NO _x + OH, hydrolysis of organic nitrates and N ₂ O ₅	Fisher et al. (2016); Wang et al. (2016)

most significant components of nitro-aromatics in the gas phase. Despite the fact that nitrated phenols could be formed by photochemical oxidation of their aromatic hydrocarbon precursors (Z. Wang et al., 2020; Yuan et al., 2016), none of them peaked in the daytime, consistent with a previous proposal on photolysis as the dominant loss pathway for

these compounds (Chen et al., 2011; Yuan et al., 2016). C₆H₅NO₃ and C₇H₇NO₃ peaked in the evening, suggesting important contributions of NO₃-induced reactions and/or primary emissions. The peak time of C₆H₄N₂O₅ was later than that of C₆H₅NO₃, in agreement with dinitrophenols as

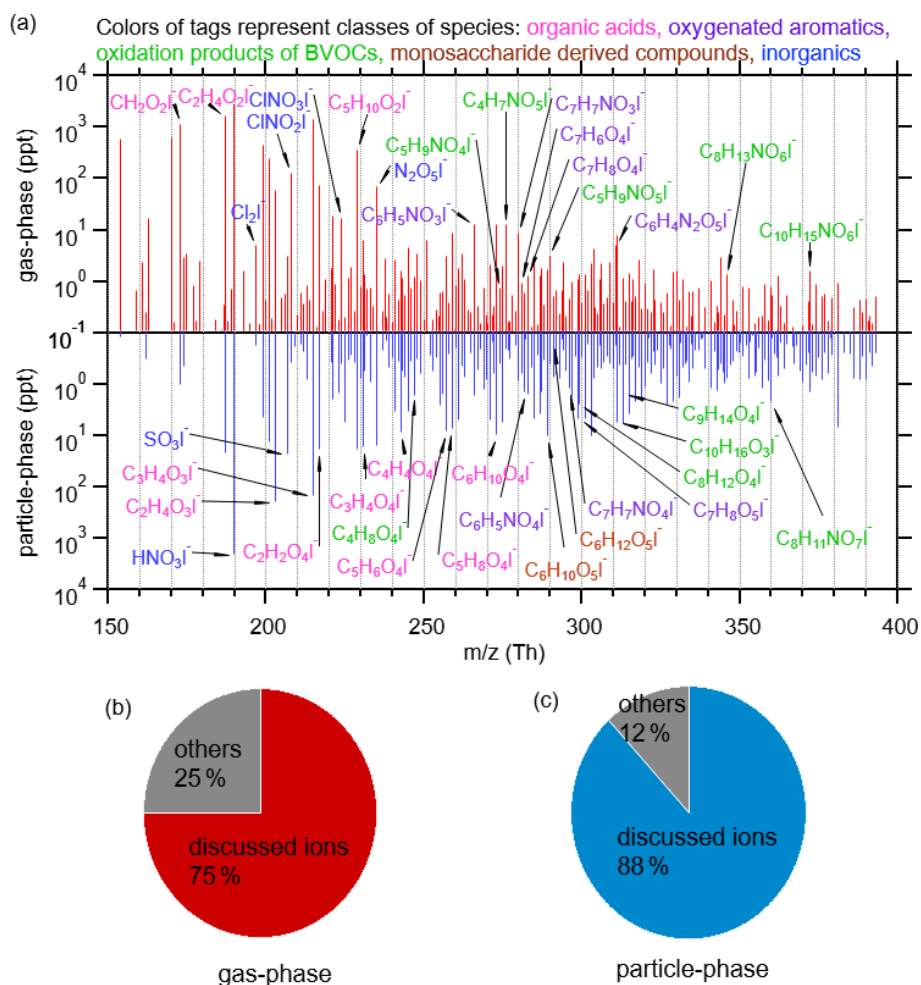


Figure 1. (a) Mass spectra of the iodide charged ion within m/z 150–400 Th in the gas phase (red) and the particle phase (blue), respectively. (b, c) The fractions of I-adduct ions discussed in the main text (Table 1) in the total ion signals for I-adduct ions measured in the gas phase (b) and the particle phase (c), respectively.

the oxidation products from nitrophenols (Harrison et al., 2005).

We also detected non-N-containing compounds that were identified as oxidation products of aromatics in the literature, including $\text{C}_7\text{H}_6\text{O}_4^-$, $\text{C}_7\text{H}_8\text{O}_4^-$ and $\text{C}_7\text{H}_8\text{O}_5^-$ (Mehra et al., 2020; Schwantes et al., 2017). $\text{C}_7\text{H}_6\text{O}_4$ and $\text{C}_7\text{H}_8\text{O}_4$ correlated well with each other ($r = 0.72$ in the gas phase and 0.91 in the particle phase). High concentrations of $\text{C}_7\text{H}_6\text{O}_4$ and $\text{C}_7\text{H}_8\text{O}_4$ were mainly observed during the periods with lower NO_x concentration, which was a contrast to the variations of nitrophenols (Fig. S10). In addition, the concentration ratios of $\text{C}_7\text{H}_8\text{O}_4^-$ and $\text{C}_7\text{H}_7\text{NO}_3^-$ are lower for higher NO_x concentration (Fig. 5), consistent with the literature stating that the formation of $\text{C}_7\text{H}_6\text{O}_4$ and $\text{C}_7\text{H}_8\text{O}_4$ is suppressed at high NO_x concentration (Schwantes et al., 2017). $\text{C}_7\text{H}_8\text{O}_5$ is reported as the ring-retaining oxidation product of $\text{C}_7\text{H}_8\text{O}_4$, which is a typical oxidation product of toluene and cresol (Schwantes et al., 2017; M. Wang et al.,

2020), as well as the ring-scission products of aromatic hydrocarbons with more carbon atoms, e.g., trimethyl benzenes (Mehra et al., 2020). Given that $\text{C}_7\text{H}_8\text{O}_5$ closely followed with $\text{C}_7\text{H}_8\text{O}_4$ ($r = 0.93$ in particles), toluene oxidation was probably the main contributor to this compound.

3.4 Organic acids and related compounds

Organic acids were one of the most abundant species classes detected by I-CIMS (Fig. 1). Low-molecular-weight organic acids (e.g., formic, acetic, glycolic and pyruvic acid) constituted a significant fraction of signals in the mass spectra of the gas phase. As shown in Fig. 6 (and also Fig. S11), they had very similar temporal trends with diurnal maxima in the afternoon, indicating photochemical oxidation played a dominant role in their formation (de Gouw et al., 2018; Yuan et al., 2015).

In contrast to monocarboxylic acids, dicarboxylic acids partitioned mostly to the particle phase. As the dominant di-

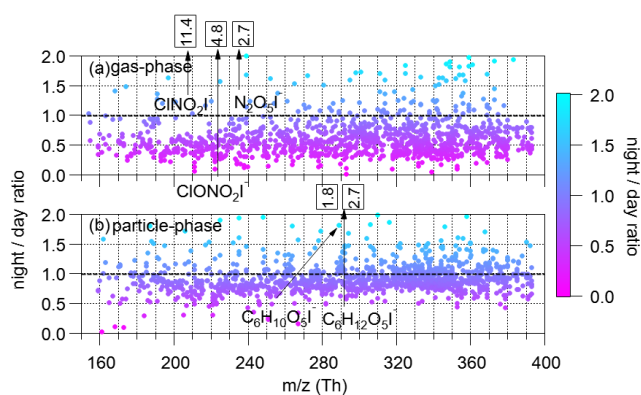


Figure 2. The ratios of concentrations at night (22:00–06:00) to concentrations during the day (10:00–18:00) for ions ranging from 150 to 400 Th in the gas phase (a) and the particle phase (b). The range of the y axis is set between 0 and 2 for clarity, although the ratios of some compounds are larger than 2. The numbers in boxes indicate the night / day ratios of tagged ions that exceeded the y-axis ranges.

carboxylic acids in aerosol (Kawamura and Bikkina, 2016; Mellouki et al., 2015), $94 \pm 5\%$ and $74 \pm 13\%$ (mean ± 1 standard deviation of F_p) of $C_2H_2O_4$ and $C_3H_4O_4$, attributed to oxalic and malonic acid, were found in the particle phase, respectively. The concentrations of $C_4H_6O_4$ were significantly lower compared to the C_2 and C_3 homologous series, but $C_5H_8O_4$ and $C_6H_{10}O_4$ had unexpected high abundance (Fig. 7). Additionally, $C_5H_8O_4$ and $C_6H_{10}O_4$ had considerable fractions in the gas phase ($45 \pm 13\%$ and $43 \pm 11\%$), which are significantly higher than their C_2 – C_3 homologous series. These two compounds were correlated well with each other in temporal variations ($r = 0.97$ and 0.91 in the gas phase and the particle phase, respectively), and their diurnal variations were different from those of oxalic and malonic acid (Fig. 6). Therefore, dicarboxylic acids may not be the dominant contributing species for the two compounds. $C_5H_8O_4$ and $C_6H_{10}O_4$ have been observed from previous studies on isoprene oxidation (Berndt et al., 2018, 2019), attributing them to epoxy hydroperoxyl carbonyl and accretion product, respectively. However, the relative contributions from these possibilities remain unclear.

In addition to the series of $C_nH_{2n-2}O_4$ (i.e., $C_2H_2O_4$, $C_3H_4O_4$), we also observed comparable concentrations of $C_nH_{2n-4}O_4$ series, especially for carbon number of 4 and 5 ($C_4H_4O_4$ and $C_5H_6O_4$). Considering the double bonds in the molecules, $C_nH_{2n-4}O_4$ should be more reactive than $C_nH_{2n-2}O_4$, suggesting there were large sources for these compounds. Previous studies have reported photooxidation of aromatics can generate $C_nH_{2n-4}O_4$, including $C_4H_4O_4$ and $C_5H_6O_4$ (Brege et al., 2018; Kawamura et al., 1996; Kawamura and Bikkina, 2016). Our measurements showed that temporal trends of $C_4H_4O_4$ and $C_5H_6O_4$ agreed well with those of aromatic hydrocarbons (Fig. S11b), and thus

oxidation of aromatics could be an important contributor to $C_nH_{2n-4}O_4$ in the urban air.

3.5 Oxidation products of biogenic VOCs

In addition to high anthropogenic emissions of aromatics, terrestrial vegetation nearby also released significant amounts of biogenic VOCs (BVOCs) (Wu et al., 2020). During the campaign, the concentrations of isoprene at noon were between 0.1 and 1.5 ppb, whereas the range of daily maxima of monoterpenes was 0.05–2.5 ppb. Hence, a number of oxidation products of BVOCs were detected (Figs. 8 and S12).

The ion $C_4H_7NO_5I^-$ was the most abundant N-containing C_4 organic compounds that was detected in the gas phase. Its daily maxima occurred in the afternoon and correlated moderately with methyl vinyl ketone (MVK) + methacrolein (MACR) measured by PTR-ToF-MS (Fig. 8b, $r = 0.58$). We consequently attributed $C_4H_7NO_5$ to MVK nitrates and MACR nitrates, which were reported as the second generation of organic nitrates formed from the oxidation of isoprene hydroxynitrates by OH in the presence of NO_x (Fisher et al., 2016; Paulot et al., 2009). Strong correlations were observed between $C_5H_9NO_4I^-$, $C_5H_9NO_5I^-$ and $C_4H_7NO_5I^-$ ($r = 0.93$ and 0.80 , respectively), which was in accordance with their similar formation pathways (Jacobs et al., 2014; Wennberg et al., 2018; Xiong et al., 2015). Hence, we expected these three compounds to be common oxidation products of isoprene in the polluted atmosphere. While in aerosol, 2-methylglyceric acid ($C_4H_8O_4$) is a commonly reported oxidation product of isoprene formed in high- NO_x conditions (Surratt et al., 2010). We observed the corresponding ion $C_4H_8O_4I^-$ contributing to OA especially in dry conditions with strong sunlight (Fig. S13). This evidence indicates that isoprene oxidation may contribute to $C_4H_8O_4$, but potential contribution from other sources cannot be ruled out in urban areas.

In terms of monoterpenes, a reasonable correlation (Fig. S14a, $r = 0.63$) was found between the ions $C_{10}H_{16}O_3I^-$ and $C_{10}H_{16}O_2H^+$ measured by PTR-ToF-MS. $C_{10}H_{16}O_2H^+$ was attributed to pinonaldehyde formed from the oxidation of monoterpenes (Glasius et al., 2000; Larsen et al., 2001; Mutzel et al., 2016). Therefore, we tentatively attribute $C_{10}H_{16}O_3I^-$ to pinonic acid and its oxocarboxylic acid isomers, which are formed via the oxidation of pinonaldehyde (Fang et al., 2017). $C_8H_{13}NO_6$ also exhibited enhanced gas-phase formation during the day as pinonic acid did. The correlation coefficient of the two compounds was 0.71. In contrast to other monoterpene nitrates, particle-phase $C_8H_{11}NO_7$ and $C_{10}H_{15}NO_6$ peaked at night and decreased during the daytime (Fig. S12), indicative of the role of NO_3 in producing organic nitrates as reported in the literature (Faxon et al., 2018). However, $C_{10}H_{15}NO_6$ in the gas phase showed a distinct diurnal profile with peak before the noon. Two possible types of compounds were pro-

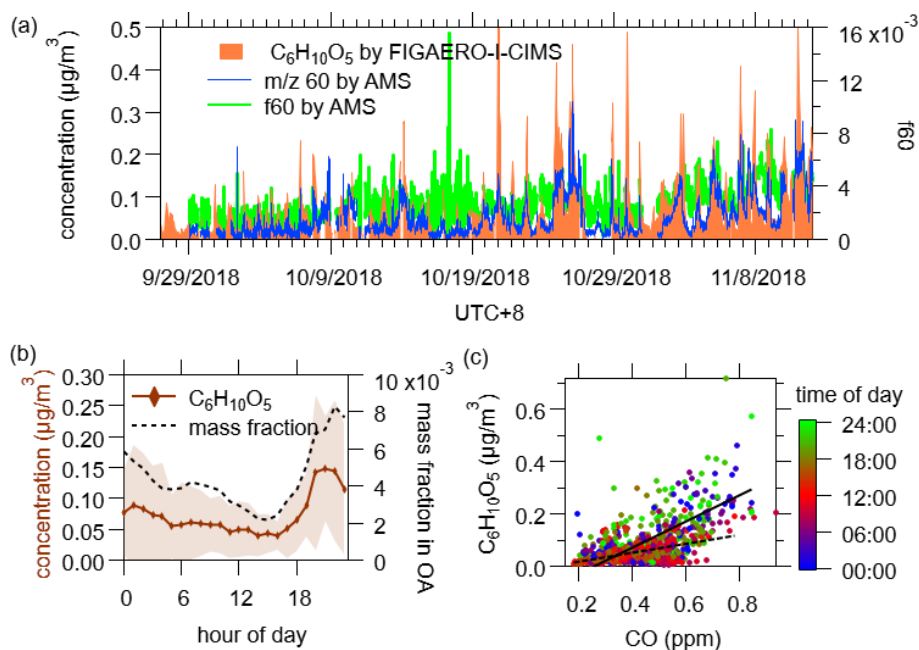


Figure 3. (a) Time series of particulate $C_6H_{10}O_5$ measured by FIGAERO-I-CIMS, m/z 60 fragment and $f60$ measured by AMS. Background $f60 = 0.3\%$ and background m/z 60 = $0.3\% \times OA$ were subtracted from $f60$ and m/z 60 (Cubison et al., 2011; Hu et al., 2016). (b) Diurnal variations of particulate $C_6H_{10}O_5$ and its mass fraction in OA. (c) Correlation between CO and particulate $C_6H_{10}O_5$. The dash and solid lines indicate the ratios during daytime (10:00–18:00, $0.17 \pm 0.02 \mu\text{g m}^{-3}/\text{ppm}$) and nighttime (22:00–06:00, $0.50 \pm 0.03 \mu\text{g m}^{-3}/\text{ppm}$), respectively.

posed for $C_{10}H_{15}NO_6$ in previous studies: peroxyacetyl nitrate from pinonaldehyde (Faxon et al., 2018; Nah et al., 2016; Schwantes et al., 2020) or organic nitrates (Bean and Hildebrandt Ruiz, 2016; Boyd et al., 2015). Given the distinct diurnal profiles of $C_{10}H_{15}NO_6I^-$ in the gas and particle phases and the fact that peroxyacetyl nitrate is supposed to dissociate during the FIGAERO heating (Slusher et al., 2004), we speculate that both compounds contributed to this ion. As shown in Fig. S15, $C_8H_{12}O_4$ and $C_9H_{14}O_4$ existed mostly in the particle phase ($F_p = 0.63 \pm 0.11$ and 0.67 ± 0.10 , respectively). We interpret them as products of monoterpenes via photochemical processes, consistent with the interpretations presented in previous work (Mohr et al., 2013; Mutzel et al., 2015).

3.6 S-containing compounds

Organosulfates are concerned as important components of SOA (Hallquist et al., 2009; Surratt et al., 2007), and they can be detected by iodide anion via proton abstraction (Le Breton et al., 2018b; Lee et al., 2014). We detected the ion $C_2H_3SO_6^-$ with a diurnal peak in the afternoon (Fig. 9). This ion was attributed to glycolic acid sulfate, as suggested by previous work (Galloway et al., 2009; Liao et al., 2015).

Abundant SO_3I^- was detected in particles, and it correlated well with the ion $C_2H_3SO_6^-$ (Fig. 9b) and sulfates measured by AMS (Fig. S16). Previous work observed the sulfate

ion radical ($^*SO_3^-$) during the ionization of organosulfates in a liquid chromatography–electrospray ionization–tandem mass spectrometer (Huang et al., 2018). As a result, the ion SO_3I^- from FIGAERO-I-CIMS might be a potential indicator for the total organosulfates. However, more future work is needed for evaluating this possibility.

Other sulfate-related ions during gas-phase modes were also detected, including HSO_4^- (sulfuric acid) and $CH_3SO_3^-$ (methanesulfonic acid), which were enhanced in the gas phase during the daytime, in agreement with the notions of photochemistry-induced gas-phase oxidation (Brandt and van Eldik, 1995). However, these data were not available for quantification given that these low-volatility species would condense on our long gas sampling inlet. It should be noted that measuring sulfuric acid in the gas phase is difficult and generally requires a “wall-less” source design (Eisele and Tanner, 1993).

3.7 Inorganic compounds

There is a growing interest in N_2O_5 and its product nitryl chloride ($ClNO_2$) because $ClNO_2$ is found to serve as a nocturnal reservoir of Cl radical and reactive nitrogen, and hence enhance the ozone formation the next day (Osthoff et al., 2008; Wang et al., 2016). Time series of N_2O_5 and $ClNO_2$ exhibited two patterns. During most of the nights, N_2O_5 started to increase quickly at sunset and lasted for

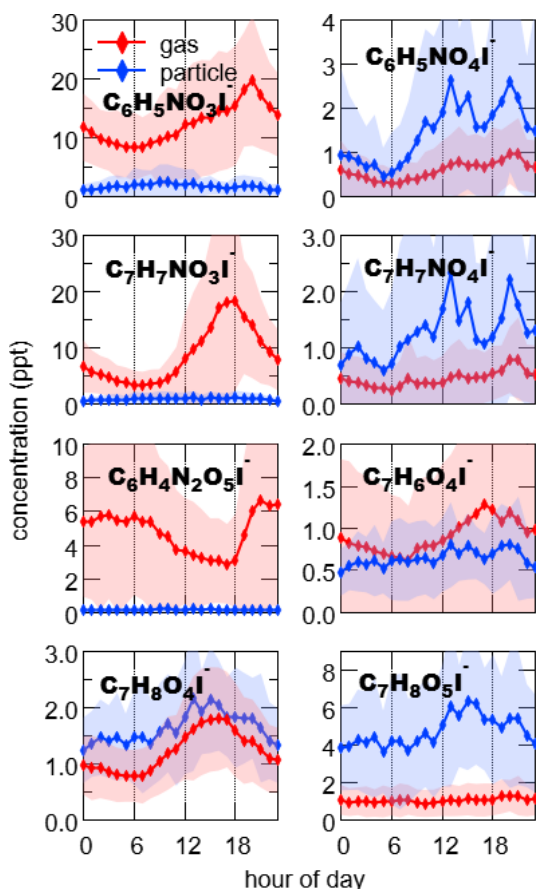


Figure 4. Diurnal variations of oxidized aromatics including nitro-phenols ($\text{C}_6\text{H}_5\text{NO}_3\text{I}^-$), nitro-benzenediols ($\text{C}_6\text{H}_5\text{NO}_4\text{I}^-$), methyl nitro-phenols ($\text{C}_7\text{H}_7\text{NO}_3\text{I}^-$), methyl nitro-benzenediols ($\text{C}_7\text{H}_7\text{NO}_4\text{I}^-$), dinitro-phenols ($\text{C}_6\text{H}_4\text{N}_2\text{O}_5\text{I}^-$), dihydroxy methyl benzoquinone ($\text{C}_7\text{H}_6\text{O}_4\text{I}^-$), tetrahydroxy toluene ($\text{C}_7\text{H}_8\text{O}_4\text{I}^-$), pentahydroxy toluene and fragments of C_9 aromatics ($\text{C}_7\text{H}_8\text{O}_5\text{I}^-$). The shaded areas indicate 1 standard deviation.

only 2–3 h, and ClNO_2 increased in the meantime and ultimately reached its maximum at night, indicative of local formation of ClNO_2 . However, sometimes a high level of N_2O_5 did not lead to an increase in ClNO_2 (tinted background in Fig. 10a), probably due to the lack of chloride salts on the aerosol. Other nocturnal species including ClONO_2 and Cl_2 were highly correlated with ClNO_2 as expected ($r = 0.92$ and 0.83 , respectively), suggesting they had common formation mechanisms (Liu et al., 2017).

HNO_3I^- was observed as one of the most abundant species in the mass spectra of FIGAERO-I-CIMS both in the gas phase and the particle phase. In the gas phase, the ion HNO_3I^- from I-CIMS has been used to quantify nitric acid (Lee et al., 2018a). The concentrations of gas-phase nitric acid peaked in the afternoon, suggesting photochemistry in the daytime as the dominant source for gas-phase nitric acid.

Previous studies suggested that HNO_3I^- from particle-phase measurement by FIGAERO-I-CIMS can be indica-

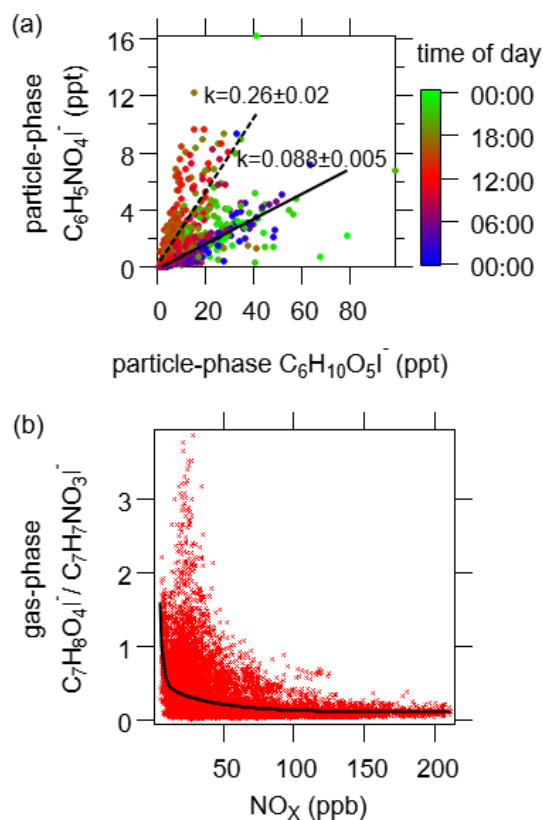


Figure 5. (a) Correlation between particle-phase $\text{C}_6\text{H}_5\text{NO}_4\text{I}^-$ and $\text{C}_6\text{H}_{10}\text{O}_5\text{I}^-$. The data points are color-coded using the time of the day. Solid and dash lines represent the slopes during the nighttime and daytime, respectively. (b) Relative concentration of $\text{C}_7\text{H}_8\text{O}_4\text{I}^-$ and $\text{C}_7\text{H}_7\text{NO}_3\text{I}^-$ in the gas phase as a function of NO_x concentration. The black line is the fitted curve using a double exponential function.

tive of nitrate in the particle phase (Lee et al., 2016). Here, the concentrations of HNO_3I^- in the particle phase were compared with particulate nitrate measured by AMS (Fig. 11c). A strong correlation was observed ($r = 0.93$), but the concentrations measured by FIGAERO-I-CIMS were higher (slope = 1.6), especially for higher concentrations of organic nitrates. Using a threshold of $1 \mu\text{g}/\text{m}^3$ for organic nitrates, the slopes and correlations were higher for the data points with particulate organic nitrates larger than $1 \mu\text{g}/\text{m}^3$ (slope = 1.8, $r = 0.94$) than those less than $1 \mu\text{g}/\text{m}^3$ (slope = 1.1, $r = 0.90$). In short, our measurements suggest that HNO_3I^- in the particle phase from FIGAERO-I-CIMS is formed from thermal decomposition of both inorganic nitrate (e.g., NH_4NO_3) and organic nitrates.

3.8 Bulk chemical properties of detected organic compounds

The above discussions on individual chemical groups provide insights into the identification of the mass spectra from FIGAERO-I-CIMS, along with sources and chemistry of

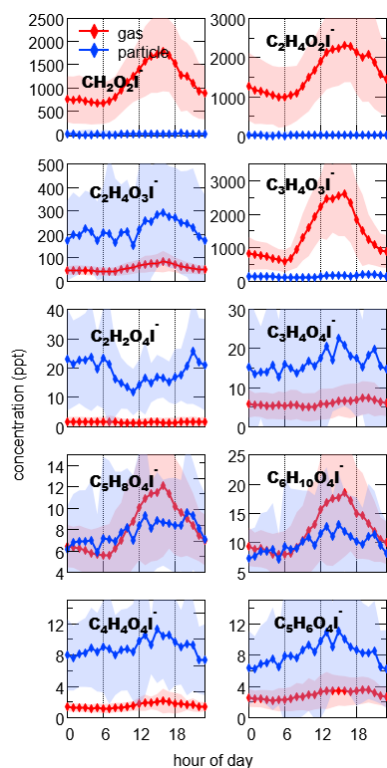


Figure 6. Diurnal variations of organic acids in the gas phase (red) and particle phase (blue). The shaded area indicates 1 standard deviation.

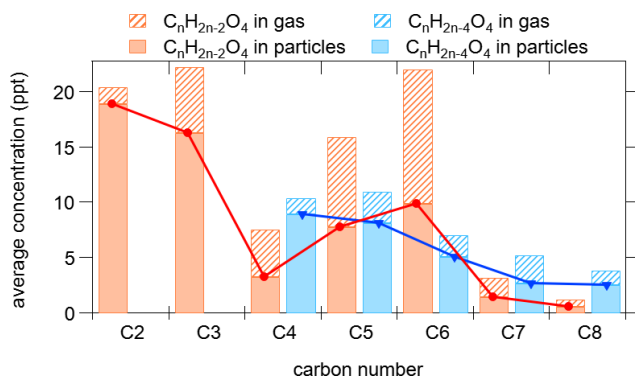


Figure 7. Average concentrations of compounds with the formulas of $C_nH_{2n-2}O_4$ and $C_nH_{2n-4}O_4$.

oxygenated organic compounds in the urban atmosphere. In this section and the following one, we will provide a bulk analysis of the detected organic compounds.

Organic compounds detected by FIGAERO-I-CIMS were comprehensively characterized with detailed elementary composition in $\overline{OS}_C - n_C$ space (Fig. 12), which depicts the average oxidation states of carbon for closed-shell $C_xH_yO_z$ and $C_xH_yN_{1,2}O_z$ compounds as a function of carbon number. The details in the calculation of \overline{OS}_C can be found in Sect. S2 in the Supplement. S-containing compounds were

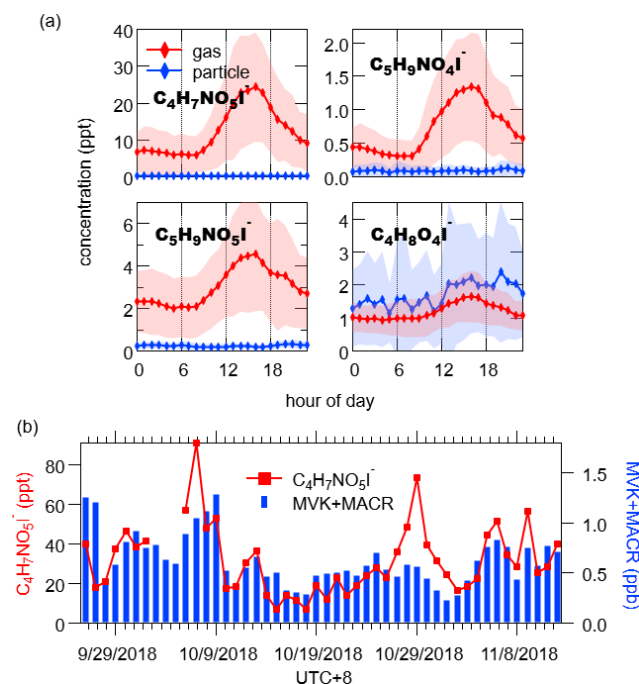


Figure 8. (a) Diurnal variations of isoprene oxidation products in the gas phase (red) and particle phase (blue). The shaded area indicates 1 standard deviation. (b) Time series of daily maximum concentrations of gaseous $C_4H_7NO_5I^-$ and MVK + MACR ($C_4H_6OH^+$, m/z 71.05) measured by PTR-ToF-MS.

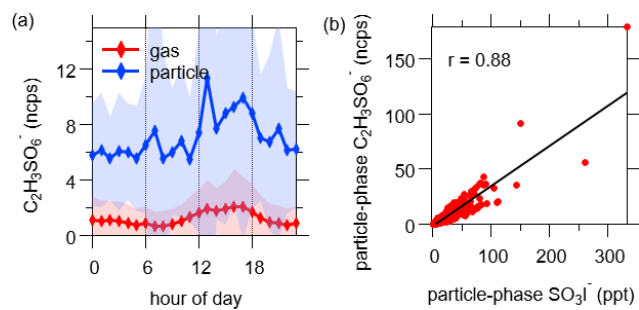


Figure 9. (a) Diurnal variation of $C_2H_3SO_6^-$. The shaded areas indicate 1 standard deviation. (b) Correlation between particle-phase $C_2H_3SO_6^-$ and SO_3I^- .

omitted given their negligible variety and concentration compared to $C_xH_yO_z$ and $C_xH_yN_{1,2}O_z$. The average \overline{OS}_C in the particle phase was higher than that in the gas phase at the same carbon number, especially for carbon numbers between 2 and 10. This agrees with our expectation that more oxidized compounds would partition more strongly in aerosol, as indicated by larger fractions in particles (F_p) for higher \overline{OS}_C . In addition, the average \overline{OS}_C generally increased for lower carbon number, as a result of functionalization and fragmentation during VOCs aging. However, there was a notable exception in C_5 which had a significantly reduced \overline{OS}_C , probably as the result of emissions of isoprene. The analysis of

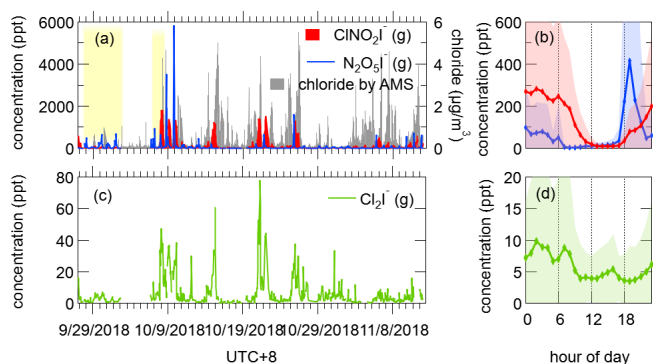


Figure 10. Time series and diurnal variations of humidity-corrected concentrations of N_2O_5 and ClNO_2 (a, b) and Cl_2 (c, d). The tinted background indicates the days with high concentrations of N_2O_5 but low concentrations of ClNO_2 . The shaded areas indicate 1 standard deviation.

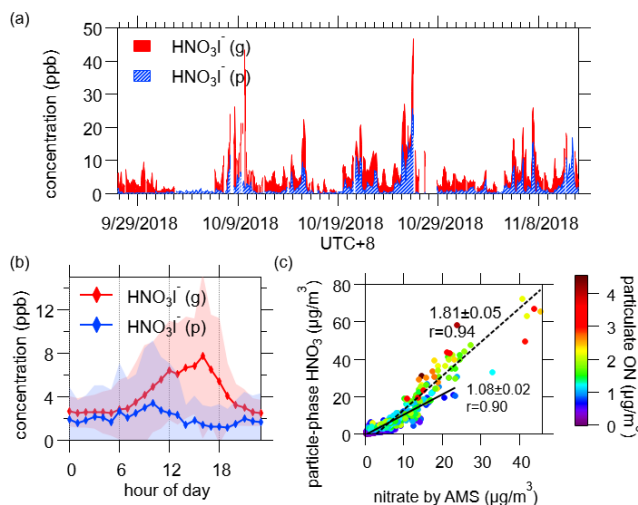


Figure 11. (a) Time series of humidity-corrected HNO_3I^- in both phases. (b) Diurnal variation of humidity-corrected HNO_3I^- . The shaded areas indicate 1 standard deviation. (c) Comparison of particle-phase HNO_3I^- and nitrate measured by AMS. The color scale denotes particulate N-containing organic compounds measured by FIGAERO-I-CIMS (pON). The solid and dash lines show the fitted results for the dataset of pON less than $1 \mu\text{g}/\text{m}^3$ and more than $1 \mu\text{g}/\text{m}^3$, respectively. The concentration of gaseous HNO_3I^- shown here only included the last 5 min of every gas-phase working mode, as high level of HNO_3 came out of aerosol, which then passed through the CIMS in a short time during particle analysis, and a substantial amount would subsequently accumulate on the inner surfaces, leading to a persistent carried over signal that was long enough to disturb the next gas measurement cycle (Palm et al., 2019).

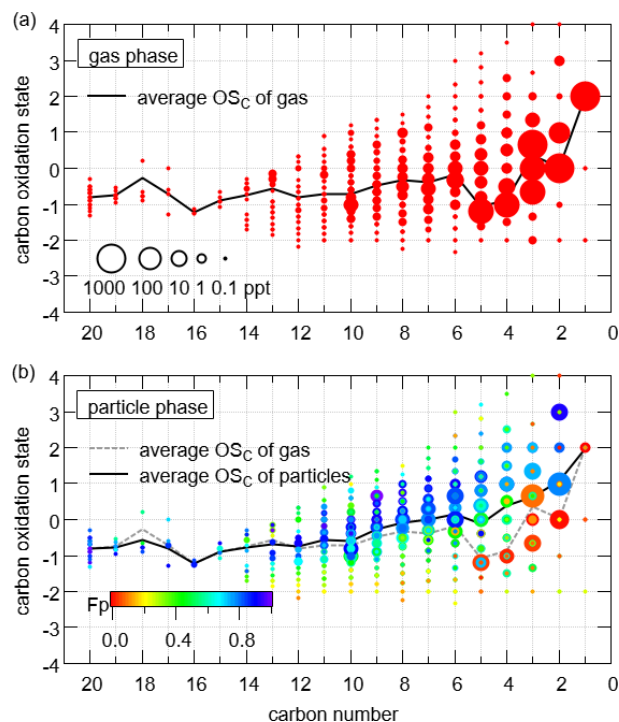


Figure 12. $\overline{\text{OS}}_C - n_C$ spaces for $\text{C}_x\text{H}_y\text{O}_z$ and $\text{C}_x\text{H}_y\text{N}_{1,2}\text{O}_z$ compounds in the gas phase (a) and the particle phase (b). The diameters of circles are proportional to the logarithmic average concentrations. The black lines are the average $\overline{\text{OS}}_C$ of each carbon number for compounds in the gas phase and the particle phase, respectively. The compounds in panel (b) are color-coded by their fractions in particles.

the $\overline{\text{OS}}_C - n_C$ space indicates that the large number of organic compounds measured by FIGAERO-I-CIMS are useful to characterize the evolution of organic compounds in the atmosphere.

The distributions of carbon and oxygen numbers of organic compounds were also investigated, as shown in Fig. 13. Most abundant organic compounds measured by FIGAERO-I-CIMS were C_2 – C_3 compounds, which accounted for about 66 % in the gas phase and 56 % in the particle phase. It is unexpected that C_2 – C_3 compounds made up such a significant portion in the particle phase, indicating a non-negligible role of thermal decomposition from low volatility compounds such as accretion products or extremely low volatility organic compounds which were reported from FIGAERO measurements on SOA (D'Ambro et al., 2018; Lopez-Hilfiker et al., 2014; Stark et al., 2017). Organic compounds with carbon numbers over five constituted only 3 % in the gas phase, while they accounted for 30 % in the particle phase. The oxygen numbers of the majority of gaseous organic compounds were no more than 3. Organic compounds containing two to three oxygen atoms had the largest contribution in both the gas phase (96 %) and the particle phase (56 %). $\text{C}_x\text{H}_y\text{N}_{1,2}\text{O}_z$ accounted for less than 10 % of the total oxygenated or-

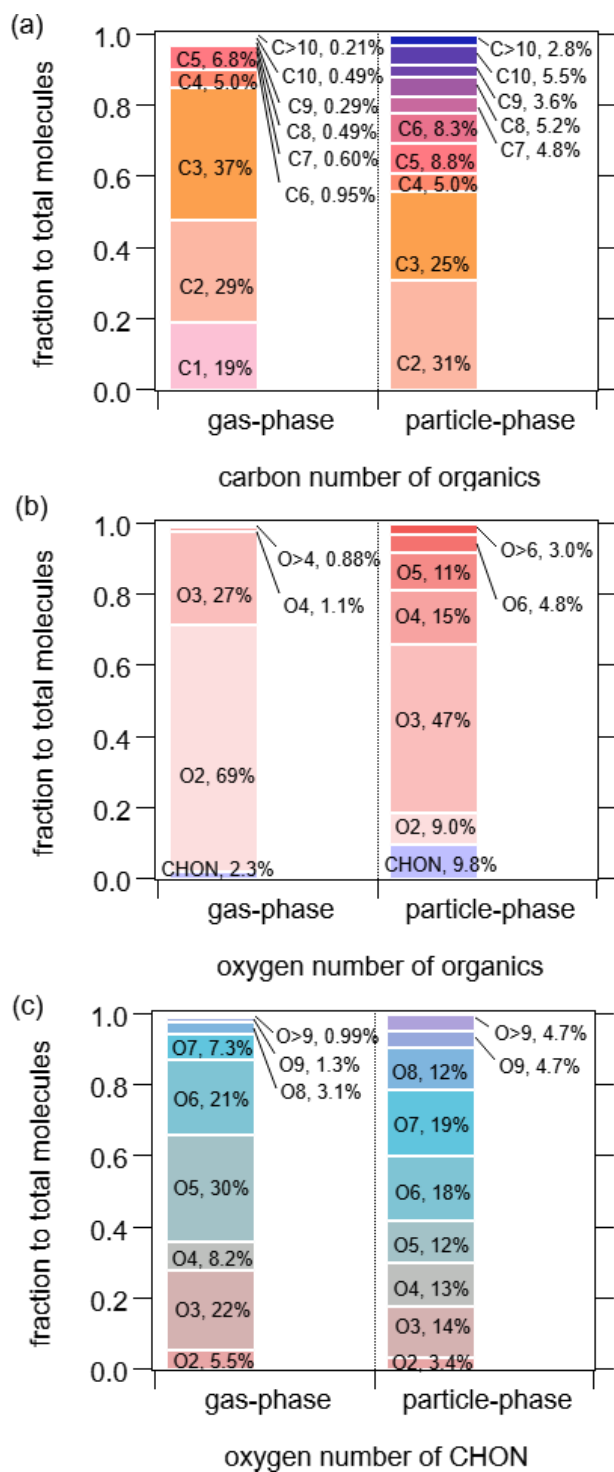


Figure 13. Carbon number distribution (a) and oxygen number distribution of total $C_xH_yO_z$ and $C_xH_yN_{1,2}O_z$ compounds (b) and oxygen number distribution of $C_xH_yN_{1,2}O_z$ compounds (c).

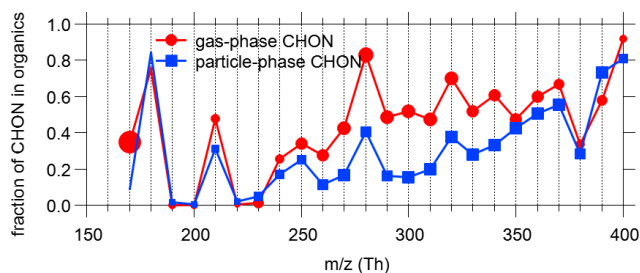


Figure 14. The average fractions of CHON to total organic compounds (CHO + CHON + CHOS + CHONS) of every 10 Th in both phases. See Fig. S16 for the overall distribution of the contributions of species classes to the total concentrations. Marker sizes indicate the total concentration level in each m/z bin. High ambient concentration of HNCO resulted in the large marker around m/z 170 in the gas phase (Z. Wang et al., 2020).

organic compounds. In the gas phase, compounds with five to six oxygen atoms accounted for 51 % of $C_xH_yN_{1,2}O_z$, indicative of the high levels of organic nitrates in the urban atmosphere. Nitrophenols also contributed significantly to $C_xH_yN_{1,2}O_z$ compounds, as they accounted for 74 % of $C_xH_yN_{1,2}O_z$ containing three oxygen atoms, which in turn contributed to 22 % of $C_xH_yN_{1,2}O_z$. In contrast, in the particle phase, the oxygen numbers of $C_xH_yN_{1,2}O_z$ distributed relatively evenly, as the fractions of compounds with three to eight oxygen atoms were similar (between 12 % and 19 %). Compared to measurements in a forest in the southeastern United States (cf., Table S1 from Lee et al., 2016), the fractions of N-containing organic compounds with less than five oxygen atoms were significantly larger in our measurements as a result of higher concentrations of nitro-aromatics.

We further determined the fractions of N-containing organic compounds in total organic compounds as a function of m/z . It is clear that the observed fractions of N-containing organic compounds were higher for elevated m/z (Fig. 14) and N-containing ions commonly dominated at even nominal masses (Fig. S17). The gas-phase CHON ions within the m/z range of 250–350 Th accounted for about half of the organic compounds in this range. The fractions of CHON ions in the particle phase were somewhat smaller than those in the gas phase within the above m/z range but were comparable for higher m/z . A possible explanation for this is that functional groups of nitrate and nitro reduce less in vapor pressure for organic compounds than functional groups of carboxylic or oxygen-equivalent hydroxyl do (Capouet and Müller, 2006; Nannoolal et al., 2008; Pankow and Asher, 2008). Consequently, CHON compounds are generally more volatile than CHO compounds with similar molecular weights.

In the end, we determined the total concentration of N-containing organic compounds in the particle phase measured by FIGAERO-I-CIMS and compared it with the particulate organic nitrates derived from AMS (Fig. 15). Good agreement was achieved when the concentration of inorganic

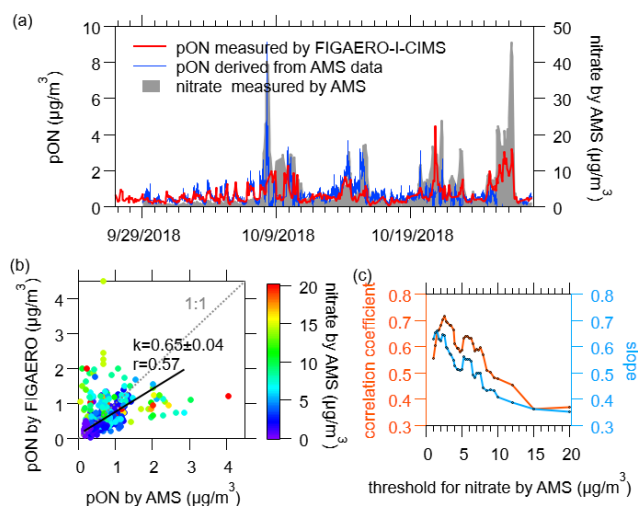


Figure 15. (a) Time series of particulate N-containing organic compounds measured by FIGAERO-I-CIMS (pON by FIGAERO), particulate organic nitrates derived from AMS data (pON by AMS) as well as particulate inorganic nitrate. (b) Comparison of pON by FIGAERO and pON by AMS, color-coded by the concentrations of particulate inorganic nitrate measured by AMS. The black line presents the linear fit for nitrate by AMS below $8 \mu\text{g}/\text{m}^3$. (c) The determined slopes and correlation coefficients between pON by FIGAERO versus pON by AMS by filtering the data below different thresholds of particulate inorganic nitrate measured by AMS.

nitrate was relatively low, e.g., below $8 \mu\text{g}/\text{m}^3$. However, the discrepancies increased when inorganic nitrate concentration increased, which can affect the determination of organic nitrate from AMS. This encouraging result indicates that FIGAERO-I-CIMS is able to capture the variability of organic nitrates in the urban atmosphere, which can be helpful in understanding the sources and formation mechanism of these compounds.

3.9 Organic aerosol measurements

The total concentration of organic compounds in the particle phase measured by FIGAERO-I-CIMS was determined and compared with measurements of OA by AMS. The total organic compounds measured by FIGAERO-I-CIMS explained $24 \pm 0.8 \%$ (fitted slope ± 1 standard deviation) of the total OA on average (Fig. 16a), which is lower than the average fractions ($\sim 50 \%$) reported previously in boreal and temperate forests (Lopez-Hilfiker et al., 2016; Stark et al., 2017). The lower fractions determined here might be the result of larger contributions to OA from primary emissions in the urban air, which are composed of a large number of compounds with little signals in I-CIMS (Zhao et al., 2016). As shown in Fig. 16a, organic compounds measured by FIGAERO-I-CIMS accounted for higher fractions in OA concentrations by AMS for more aged OA, consistent with the fact that I-CIMS is more sensitive to oxygenated organic compounds

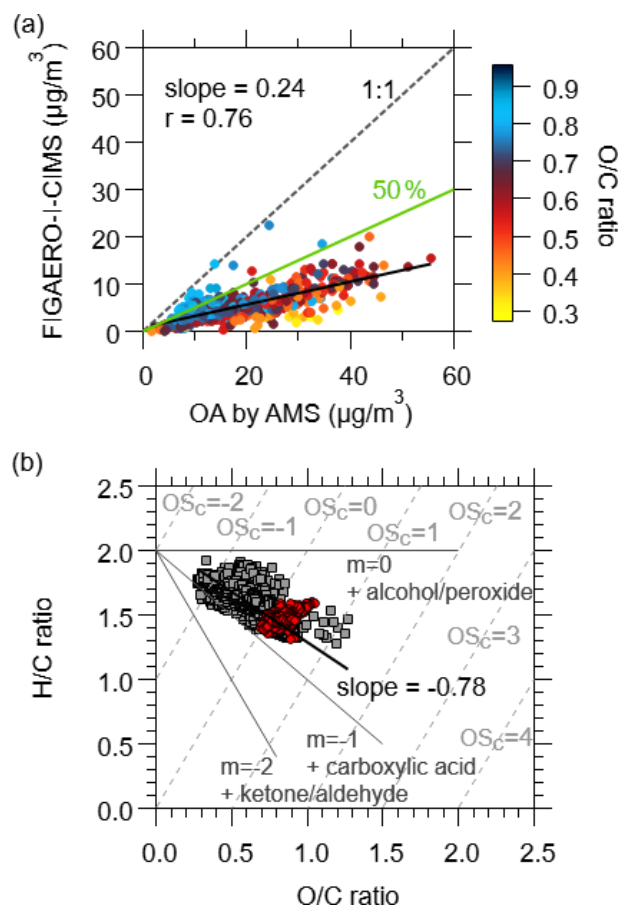


Figure 16. (a) Comparison of particulate organic compounds measured by the FIGAERO-I-CIMS and AMS, color-coded by O/C ratios measured by AMS. The black line is the slope which represents the fraction of OA explained by the measurements of FIGAERO-I-CIMS. The green line shows the results from previous work which were $\sim 50 \%$ (Lopez-Hilfiker et al., 2016; Stark et al., 2017). (b) Van Krevelen diagrams for organic aerosol derived from AMS data (gray squares) and FIGAERO-I-CIMS data (red circles). The black line is the slope of AMS data. The gray dotted lines are estimated carbon oxidation state.

with multiple functional groups (Lee et al., 2014; Lopez-Hilfiker et al., 2016). Furthermore, we expect this fraction to change with the relative contributions of primary emissions and secondary formation for organic compounds in the atmosphere. Similar trends were found in Le Breton et al. (2019), in which an acetate source was used. Acetate ions have been reported to selectively ionize highly oxygenated organic compounds as an iodide source does (Aljawhary et al., 2013).

Comparison of the van Krevelen diagrams between FIGAERO-I-CIMS and AMS also provides useful insights on the measurement of organic compounds in OA. The van Krevelen diagram has been used as a tool for analyzing functional groups and OA aging by plotting H/C ratios versus O/C ratios (Heald et al., 2010; Lambe et al.,

2012). As shown in Fig. 16b, the data points of the bulk OA from FIGAERO-I-CIMS followed the same trend as the data points from AMS. However, the bulk OA measured by FIGAERO-I-CIMS only occupied a much smaller region with O/C ratios between 0.7 and 1.0. We further plotted all of the organic compounds in the H/C versus O/C space color-coded with their campaign-average concentrations (Fig. S18a). We observed that most data points from FIGAERO-I-CIMS distributed across the zone between the slope of 0 and -1.0 . These observations provide additional evidence that FIGAERO-I-CIMS may only measure the more oxidized organic compounds in OA.

The correlation coefficients between the particle-phase concentrations at unit masses by FIGAERO-I-CIMS and OA mass concentration by AMS were calculated (Fig. S18b). The correlation coefficients were small for ions below m/z 200, as these ions contributed little to organic aerosol. Moderate and strong correlations ($r > 0.7$) were observed for the ions of m/z between 200 and 400 Th, implying that organic compounds with molecular weights of 100–300 g/mol may account for significant fractions in organic aerosol. The possible reason for the lower correlations for heavier compounds ($m/z > 400$ Th) with OA mass loadings is that these compounds might be related to specific sources or certain chemical processes, which might not contribute in large fractions to the total OA concentration.

4 Summary

We deployed a FIGAERO-I-CIMS instrument to measure oxygenated organic compounds in both the gas phase and the particle phase at a representative urban site in China. The experimental design and instrumentation setup were described in detail, which goes above and beyond typical studies, including (1) performing sensitivity calibrations in the laboratory using multiple methods for multiple species; (2) performing voltage scanning for unknown compounds detected in the ambient air; and (3) performing humidity calibrations for multiple types of species, which we have not seen anyone do after Lee et al. (2014).

From the mass spectra, a number of important compounds in the urban atmosphere were identified. We detected high concentrations of several monosaccharide species (e.g., levoglucosan). They were potentially emitted from biomass burning, which also contributed to the enhancement of many nitro-aromatic species. Photochemistry was also found to be a strong source of nitro-aromatics. Low-molecular-weight organic acids were mainly observed in the gas phase, and observations supported daytime photochemistry as the dominant source. Different diurnal profiles for various BVOC-derived organic nitrates were observed, reflecting their different formation pathways related to NO_x chemistry (i.e., daytime photooxidation, nocturnal NO_3 reactions). Local formation of nitryl chloride was observed, highlighting the

potential importance of nighttime chemistry in the urban region. Our measurements show that oxygenated organic compounds dominated the majority of detected species by FIGAERO-I-CIMS, in which CHO and CHON compounds both accounted for significant fractions. Nitrogen-containing organic compounds occupied a significant fraction of the total signals in both the gas and particle phases, with elevated fractions at higher molecular weights. The most abundant organic compounds were formic acid and multifunctional organic compounds containing three to five oxygen atoms. Organic compounds containing two to three carbon atoms accounted for over half of the total organic compounds in both the gas phase and the particle phase measured by FIGAERO-I-CIMS. During the campaign, the FIGAERO-I-CIMS measurements explained $24 \pm 0.8\%$ of OA mass measured by AMS, but the fractions were higher for more aged organic aerosol. This evidence, along with the analysis of the van Krevelen plot, indicates that FIGAERO-I-CIMS is measuring the more oxidized fraction of OA in the urban air.

Our observations suggest that oxygenated organic compounds in urban environments are complicated in both sources and chemistry. Oxygenated organic compounds can be both emitted from various emission sources (e.g., vehicular emissions and biomass burning) and also secondarily produced in the atmosphere. The chemistry in forming and removing these oxygenated organic compounds can be associated with daytime and nocturnal reactions initiated by both anthropogenic and biogenic precursors with strong influences from NO_x chemistry. This work demonstrates that the rich information in both gas and particle phases provided by FIGAERO-I-CIMS can greatly promote the understanding of emission and chemistry of organic carbon in the atmosphere of urban regions.

Data availability. The more detailed data can be provided by contacting the corresponding authors.

Supplement. The supplement related to this article is available online at: <https://doi.org/10.5194/acp-21-8455-2021-supplement>.

Author contributions. BY and MS designed the research. CSY, YL, ZLW, TGL, WWH, WC, CHW, CMW, SH, JPQ, BLW, CW, WS, XMW, ZYZ and XMW contributed to data collection. CSY performed the data analysis with contributions from WWH and WC. CSY and BY prepared the manuscript with contributions from JEK and other authors. All the authors reviewed the manuscript.

Competing interests. The authors declare that they have no conflict of interest.

Acknowledgements. The authors would like to thank Felipe Lopez-Hilfiker for helping to tune the CIMS instrument. The authors appreciate valuable comments from four anonymous reviewers.

Financial support. This research has been supported by the National Natural Science Foundation of China (grant no. 41877302), National Key R&D Plan of China (grant nos. 2019YFE0106300, 2018YFC0213904, 2016YFC0202206), Guangdong Natural Science Funds for Distinguished Young Scholar (grant no. 2018B030306037), Guangdong Provincial Key R&D Plan (grant no. 2019B110206001), Guangdong Soft Science Research Program (grant no. 2019B101001005), and Guangdong Innovative and Entrepreneurial Research Team Program (grant no. 2016ZT06N263). Weiwei Hu and Wei Chen were supported by the National Natural Science Foundation of China (grant no. 41875156), Natural Science Foundation of Guangdong (grant no. 2019A1515011153) and Guangdong Pearl River Talents Program (grant no. 2019QN01L948). This work was also supported by the Special Fund Project for Science and Technology Innovation Strategy of Guangdong Province (grant no. 2019B121205004).

Review statement. This paper was edited by Arthur Chan and reviewed by four anonymous referees.

References

- Aiken, A. C., DeCarlo, P. F., and Jimenez, J. L.: Elemental Analysis of Organic Species with Electron Ionization High-Resolution Mass Spectrometry, *Anal. Chem.*, 79, 8350–8358, <https://doi.org/10.1021/ac071150w>, 2007.
- Aljawhary, D., Lee, A. K. Y., and Abbatt, J. P. D.: High-resolution chemical ionization mass spectrometry (ToF-CIMS): application to study SOA composition and processing, *Atmos. Meas. Tech.*, 6, 3211–3224, <https://doi.org/10.5194/amt-6-3211-2013>, 2013.
- Bean, J. K. and Hildebrandt Ruiz, L.: Gas–particle partitioning and hydrolysis of organic nitrates formed from the oxidation of α -pinene in environmental chamber experiments, *Atmos. Chem. Phys.*, 16, 2175–2184, <https://doi.org/10.5194/acp-16-2175-2016>, 2016.
- Berndt, T., Scholz, W., Mentler, B., Fischer, L., Herrmann, H., Kulmala, M., and Hansel, A.: Accretion Product Formation from Self- and Cross-Reactions of RO₂ Radicals in the Atmosphere, *Angew. Chem. Int. Edit.*, 57, 3820–3824, <https://doi.org/10.1002/anie.201710989>, 2018.
- Berndt, T., Hyttinen, N., Herrmann, H., and Hansel, A.: First oxidation products from the reaction of hydroxyl radicals with isoprene for pristine environmental conditions, *Commun. Chem.*, 2, 1–10, <https://doi.org/10.1038/s42004-019-0120-9>, 2019.
- Bertram, T. H., Thornton, J. A., and Riedel, T. P.: An experimental technique for the direct measurement of N₂O₅ reactivity on ambient particles, *Atmos. Meas. Tech.*, 2, 231–242, <https://doi.org/10.5194/amt-2-231-2009>, 2009.
- Bertram, T. H., Kimmel, J. R., Crisp, T. A., Ryder, O. S., Yatavelli, R. L. N., Thornton, J. A., Cubison, M. J., Gonin, M., and Worsnop, D. R.: A field-deployable, chemical ionization time-of-flight mass spectrometer, *Atmos. Meas. Tech.*, 4, 1471–1479, <https://doi.org/10.5194/amt-4-1471-2011>, 2011.
- Bhattacharai, H., Saikawa, E., Wan, X., Zhu, H., Ram, K., Gao, S., Kang, S., Zhang, Q., Zhang, Y., Wu, G., Wang, X., Kawamura, K., Fu, P., and Cong, Z.: Levoglucosan as a tracer of biomass burning: Recent progress and perspectives, *Atmos. Res.*, 220, 20–33, <https://doi.org/10.1016/j.atmosres.2019.01.004>, 2019.
- Boyd, C. M., Sanchez, J., Xu, L., Eugene, A. J., Nah, T., Tuet, W. Y., Guzman, M. I., and Ng, N. L.: Secondary organic aerosol formation from the β -pinene + NO₃ system: effect of humidity and peroxy radical fate, *Atmos. Chem. Phys.*, 15, 7497–7522, <https://doi.org/10.5194/acp-15-7497-2015>, 2015.
- Brandt, C. and van Eldik, R.: Transition Metal-Catalyzed Oxidation of Sulfur(IV) Oxides. Atmospheric-Relevant Processes and Mechanisms, *Chem. Rev.*, 95, 119–190, <https://doi.org/10.1021/cr00033a006>, 1995.
- Brege, M., Paglione, M., Gilardoni, S., Decesari, S., Facchini, M. C., and Mazzoleni, L. R.: Molecular insights on aging and aqueous-phase processing from ambient biomass burning emissions-influenced Po Valley fog and aerosol, *Atmos. Chem. Phys.*, 18, 13197–13214, <https://doi.org/10.5194/acp-18-13197-2018>, 2018.
- Canagaratna, M. R., Jimenez, J. L., Kroll, J. H., Chen, Q., Kessler, S. H., Massoli, P., Hildebrandt Ruiz, L., Fortner, E., Williams, L. R., Wilson, K. R., Surratt, J. D., Donahue, N. M., Jayne, J. T., and Worsnop, D. R.: Elemental ratio measurements of organic compounds using aerosol mass spectrometry: characterization, improved calibration, and implications, *Atmos. Chem. Phys.*, 15, 253–272, <https://doi.org/10.5194/acp-15-253-2015>, 2015.
- Capouet, M. and Müller, J.-F.: A group contribution method for estimating the vapour pressures of α -pinene oxidation products, *Atmos. Chem. Phys.*, 6, 1455–1467, <https://doi.org/10.5194/acp-6-1455-2006>, 2006.
- Carlton, A. G., Turpin, B. J., Altieri, K. E., Seitzinger, S., Reff, A., Lim, H.-J., and Ervens, B.: Atmospheric oxalic acid and SOA production from glyoxal: Results of aqueous photooxidation experiments, *Atmos. Environ.*, 41, 7588–7602, <https://doi.org/10.1016/j.atmosenv.2007.05.035>, 2007.
- Carlsaw, N.: A mechanistic study of limonene oxidation products and pathways following cleaning activities, *Atmos. Environ.*, 80, 507–513, <https://doi.org/10.1016/j.atmosenv.2013.08.034>, 2013.
- Chen, H. and Finlayson-Pitts, B. J.: New Particle Formation from Methanesulfonic Acid and Amines/Ammonia as a Function of Temperature, *Environ. Sci. Technol.*, 51, 243–252, <https://doi.org/10.1021/acs.est.6b04173>, 2017.
- Chen, J., Wenger, J. C., and Venables, D. S.: Near-Ultraviolet Absorption Cross Sections of Nitrophenols and Their Potential Influence on Tropospheric Oxidation Capacity, *J. Phys. Chem. A*, 115, 12235–12242, <https://doi.org/10.1021/jp206929r>, 2011.
- Cubison, M. J., Ortega, A. M., Hayes, P. L., Farmer, D. K., Day, D., Lechner, M. J., Brune, W. H., Apel, E., Diskin, G. S., Fisher, J. A., Fuelberg, H. E., Hecobian, A., Knapp, D. J., Mikoviny, T., Riemer, D., Sachse, G. W., Sessions, W., Weber, R. J., Weinheimer, A. J., Wisthaler, A., and Jimenez, J. L.: Effects of aging on organic aerosol from open biomass burning smoke in aircraft and laboratory studies, *Atmos. Chem. Phys.*, 11, 12049–12064, <https://doi.org/10.5194/acp-11-12049-2011>, 2011.
- D'Ambro, E. L., Lee, B. H., Liu, J., Shilling, J. E., Gaston, C. J., Lopez-Hilfiker, F. D., Schobesberger, S., Zaveri, R. A., Mohr,

- C., Lutz, A., Zhang, Z., Gold, A., Surratt, J. D., Rivera-Rios, J. C., Keutsch, F. N., and Thornton, J. A.: Molecular composition and volatility of isoprene photochemical oxidation secondary organic aerosol under low- and high-NO_x conditions, *Atmos. Chem. Phys.*, 17, 159–174, <https://doi.org/10.5194/acp-17-159-2017>, 2017.
- D'Ambro, E. L., Schobesberger, S., Zaveri, R. A., Shilling, J. E., Lee, B. H., Lopez-Hilfiker, F. D., Mohr, C., and Thornton, J.: Isothermal evaporation of α -pinene ozonolysis SOA: volatility, phase state, and oligomeric composition, *ACS Earth Sp. Chem.*, 2, 1058–1067, <https://doi.org/10.1021/acsearthspacechem.8b00084>, 2018.
- de Gouw, J. A., Middlebrook, A. M., Warneke, C., Goldan, P. D., Kuster, W. C., Roberts, J. M., Fehsenfeld, F. C., Worsnop, D. R., Canagaratna, M. R., Pszenny, A. A. P., Keene, W. C., Marchewka, M., Bertman, S. B., and Bates, T. S.: Budget of organic carbon in a polluted atmosphere: Results from the New England Air Quality Study in 2002, *J. Geophys. Res.-Atmos.*, 110, 1–22, <https://doi.org/10.1029/2004JD005623>, 2005.
- de Gouw, J. A., Gilman, J. B., Kim, S. W., Alvarez, S. L., Dusanter, S., Graus, M., Griffith, S. M., Isaacman-VanWertz, G., Kuster, W. C., Lefer, B. L., Lerner, B. M., McDonald, B. C., Rappenglück, B., Roberts, J. M., Stevens, P. S., Stutz, J., Thalman, R., Veres, P. R., Volkamer, R., Warneke, C., Washenfelder, R. A., and Young, C. J.: Chemistry of Volatile Organic Compounds in the Los Angeles Basin: Formation of Oxygenated Compounds and Determination of Emission Ratios, *J. Geophys. Res.-Atmos.*, 123, 2298–2319, <https://doi.org/10.1002/2017JD027976>, 2018.
- Edwards, P. M., Brown, S. S., Roberts, J. M., Ahmadov, R., Banta, R. M., DeGouw, J. A., Dubé, W. P., Field, R. A., Flynn, J. H., Gilman, J. B., Graus, M., Helmig, D., Koss, A., Langford, A. O., Lefer, B. L., Lerner, B. M., Li, R., Li, S. M., McKeen, S. A., Murphy, S. M., Parrish, D. D., Senff, C. J., Soltis, J., Stutz, J., Sweeney, C., Thompson, C. R., Trainer, M. K., Tsai, C., Veres, P. R., Washenfelder, R. A., Warneke, C., Wild, R. J., Young, C. J., Yuan, B., and Zamora, R.: High winter ozone pollution from carbonyl photolysis in an oil and gas basin, *Nature*, 514, 351–354, <https://doi.org/10.1038/nature13767>, 2014.
- Eger, P. G., Schuladen, J., Sobanski, N., Fischer, H., Karu, E., Williams, J., Riva, M., Zha, Q., Ehn, M., Quéléver, L. L. J., Schallhart, S., Lelieveld, J., and Crowley, J. N.: Pyruvic acid in the boreal forest: gas-phase mixing ratios and impact on radical chemistry, *Atmos. Chem. Phys.*, 20, 3697–3711, <https://doi.org/10.5194/acp-20-3697-2020>, 2020.
- Eisele, F. L. and Tanner, D. J.: Measurement of the gas phase concentration of H₂SO₄ and methane sulfonic acid and estimates of H₂SO₄ production and loss in the atmosphere, *J. Geophys. Res.-Atmos.*, 98, 9001–9010, <https://doi.org/10.1029/93JD00031>, 1993.
- Fang, W., Gong, L., and Sheng, L.: Online analysis of secondary organic aerosols from OH-initiated photooxidation and ozonolysis of α -pinene, β -pinene, Δ 3-carene and d-limonene by thermal desorption-photoionisation aerosol mass spectrometry, *Environ. Chem.*, 14, 75–90, <https://doi.org/10.1071/EN16128>, 2017.
- Faxon, C., Hammes, J., Le Breton, M., Pathak, R. K., and Hallquist, M.: Characterization of organic nitrate constituents of secondary organic aerosol (SOA) from nitrate-radical-initiated oxidation of limonene using high-resolution chemical ionization mass spectrometry, *Atmos. Chem. Phys.*, 18, 5467–5481, <https://doi.org/10.5194/acp-18-5467-2018>, 2018.
- Fisher, J. A., Jacob, D. J., Travis, K. R., Kim, P. S., Marais, E. A., Chan Miller, C., Yu, K., Zhu, L., Yantosca, R. M., Sulprizio, M. P., Mao, J., Wennberg, P. O., Crouse, J. D., Teng, A. P., Nguyen, T. B., St. Clair, J. M., Cohen, R. C., Romer, P., Nault, B. A., Wooldridge, P. J., Jimenez, J. L., Campuzano-Jost, P., Day, D. A., Hu, W., Shepson, P. B., Xiong, F., Blake, D. R., Goldstein, A. H., Misztal, P. K., Hanisco, T. F., Wolfe, G. M., Ryerson, T. B., Wisthaler, A., and Mikoviny, T.: Organic nitrate chemistry and its implications for nitrogen budgets in an isoprene- and monoterpene-rich atmosphere: constraints from aircraft (SEAC⁴RS) and ground-based (SOAS) observations in the Southeast US, *Atmos. Chem. Phys.*, 16, 5969–5991, <https://doi.org/10.5194/acp-16-5969-2016>, 2016.
- Fountoukis, C. and Nenes, A.: ISORROPIA II: a computationally efficient thermodynamic equilibrium model for K⁺–Ca²⁺–Mg²⁺–NH₄⁺–Na⁺–SO₄²⁻–NO₃⁻–Cl–H₂O aerosols, *Atmos. Chem. Phys.*, 7, 4639–4659, <https://doi.org/10.5194/acp-7-4639-2007>, 2007.
- Fry, J. L., Draper, D. C., Zarzana, K. J., Campuzano-Jost, P., Day, D. A., Jimenez, J. L., Brown, S. S., Cohen, R. C., Kaser, L., Hansel, A., Cappellin, L., Karl, T., Hodzic Roux, A., Turnipseed, A., Cantrell, C., Lefer, B. L., and Grossberg, N.: Observations of gas- and aerosol-phase organic nitrates at BEACHON-RoMBAS 2011, *Atmos. Chem. Phys.*, 13, 8585–8605, <https://doi.org/10.5194/acp-13-8585-2013>, 2013.
- Galloway, M. M., Chhabra, P. S., Chan, A. W. H., Surratt, J. D., Flagan, R. C., Seinfeld, J. H., and Keutsch, F. N.: Glyoxal uptake on ammonium sulphate seed aerosol: reaction products and reversibility of uptake under dark and irradiated conditions, *Atmos. Chem. Phys.*, 9, 3331–3345, <https://doi.org/10.5194/acp-9-3331-2009>, 2009.
- Gaston, C. J., Lopez-Hilfiker, F. D., Whybrew, L. E., Hadley, O., McNair, F., Gao, H., Jaffe, D. A., and Thornton, J. A.: Online molecular characterization of fine particulate matter in Port Angeles, WA: Evidence for a major impact from residential wood smoke, *Atmos. Environ.*, 138, 99–107, <https://doi.org/10.1016/j.atmosenv.2016.05.013>, 2016.
- Glasius, M., Lahaniati, M., Calogirou, A., Di Bella, D., Jensen, N. R., Hjorth, J., Kotzias, D., and Larsen, B. R.: Carboxylic acids in secondary aerosols from oxidation of cyclic monoterpenes by ozone, *Environ. Sci. Technol.*, 34, 1001–1010, <https://doi.org/10.1021/es990445r>, 2000.
- Gondwe, M., Krol, M., Gieskes, W., Klaassen, W., and de Baar, H.: The contribution of ocean-leaving DMS to the global atmospheric burdens of DMS, MSA, SO₂, and NSS SO₄⁼, *Global Biogeochem. Cy.*, 17, 1056, <https://doi.org/10.1029/2002GB001937>, 2003.
- Guo, H., Xu, L., Bougiatioti, A., Cerully, K. M., Capps, S. L., Hite Jr., J. R., Carlton, A. G., Lee, S.-H., Bergin, M. H., Ng, N. L., Nenes, A., and Weber, R. J.: Fine-particle water and pH in the southeastern United States, *Atmos. Chem. Phys.*, 15, 5211–5228, <https://doi.org/10.5194/acp-15-5211-2015>, 2015.
- Hallquist, M., Wenger, J. C., Baltensperger, U., Rudich, Y., Simpson, D., Claeys, M., Dommen, J., Donahue, N. M., George, C., Goldstein, A. H., Hamilton, J. F., Herrmann, H., Hoffmann, T., Iinuma, Y., Jang, M., Jenkin, M. E., Jimenez, J. L., Kiendler-Scharr, A., Maenhaut, W., McFiggans, G., Mentel, Th.

- F., Monod, A., Prévôt, A. S. H., Seinfeld, J. H., Surratt, J. D., Szmigielski, R., and Wildt, J.: The formation, properties and impact of secondary organic aerosol: current and emerging issues, *Atmos. Chem. Phys.*, 9, 5155–5236, <https://doi.org/10.5194/acp-9-5155-2009>, 2009.
- Hammes, J., Lutz, A., Mentel, T., Faxon, C., and Hallquist, M.: Carboxylic acids from limonene oxidation by ozone and hydroxyl radicals: insights into mechanisms derived using a FIGAERO-CIMS, *Atmos. Chem. Phys.*, 19, 13037–13052, <https://doi.org/10.5194/acp-19-13037-2019>, 2019.
- Harrison, M. A. J., Barra, S., Borghesi, D., Vione, D., Arsene, C., and Iulian Olariu, R.: Nitrated phenols in the atmosphere: a review, *Atmos. Environ.*, 39, 231–248, <https://doi.org/10.1016/j.atmosenv.2004.09.044>, 2005.
- He, Q.-F., Ding, X., Wang, X.-M., Yu, J.-Z., Fu, X.-X., Liu, T.-Y., Zhang, Z., Xue, J., Chen, D.-H., Zhong, L.-J., and Donahue, N. M.: Organosulfates from Pinene and Isoprene over the Pearl River Delta, South China: Seasonal Variation and Implication in Formation Mechanisms, *Environ. Sci. Technol.*, 48, 9236–9245, <https://doi.org/10.1021/es501299v>, 2014.
- Heald, C. L., Kroll, J. H., Jimenez, J. L., Docherty, K. S., Decarlo, P. F., Aiken, A. C., Chen, Q., Martin, S. T., Farmer, D. K., and Artaxo, P.: A simplified description of the evolution of organic aerosol composition in the atmosphere, *Geophys. Res. Lett.*, 37, L08803, <https://doi.org/10.1029/2010GL042737>, 2010.
- Hodzic, A., Jimenez, J. L., Madronich, S., Canagaratna, M. R., Decarlo, P. F., Kleinman, L., and Fast, J.: Modeling organic aerosols in a megacity: potential contribution of semi-volatile and intermediate volatility primary organic compounds to secondary organic aerosol formation, *Atmos. Chem. Phys.*, 10, 5491–5514, <https://doi.org/10.5194/acp-10-5491-2010>, 2010.
- Hu, W., Hu, M., Hu, W., Jimenez, J. L., Yuan, B., Chen, W., Wang, M., Wu, Y., Chen, C., Wang, Z., Peng, J., Zeng, L., and Shao, M.: Chemical composition, sources, and aging process of submicron aerosols in Beijing: Contrast between summer and winter, *J. Geophys. Res.-Atmos.*, 121, 1955–1977, <https://doi.org/10.1002/2015JD024020>, 2016.
- Hu, W., Day, D. A., Campuzano-Jost, P., Nault, B. A., Park, T., Lee, T., Croteau, P., Canagaratna, M. R., Jayne, J. T., Worsnop, D. R., and Jimenez, J. L.: Evaluation of the new capture vaporizer for aerosol mass spectrometers: Characterization of organic aerosol mass spectra, *Aerosol Sci. Tech.*, 52, 725–739, <https://doi.org/10.1080/02786826.2018.1454584>, 2018.
- Huang, R. J., Zhang, Y., Bozzetti, C., Ho, K. F., Cao, J. J., Han, Y., Daellenbach, K. R., Slowik, J. G., Platt, S. M., Canonaco, F., Zotter, P., Wolf, R., Pieber, S. M., Bruns, E. A., Crippa, M., Ciarelli, G., Piazzalunga, A., Schwikowski, M., Abbaszade, G., Schnelle-Kreis, J., Zimmermann, R., An, Z., Szidat, S., Baltensperger, U., El Haddad, I., and Prévôt, A. S. H.: High secondary aerosol contribution to particulate pollution during haze events in China, *Nature*, 514, 218–222, <https://doi.org/10.1038/nature13774>, 2015.
- Huang, R.-J., Cao, J., Chen, Y., Yang, L., Shen, J., You, Q., Wang, K., Lin, C., Xu, W., Gao, B., Li, Y., Chen, Q., Hoffmann, T., O’Dowd, C. D., Bilde, M., and Glasius, M.: Organosulfates in atmospheric aerosol: synthesis and quantitative analysis of PM_{2.5} from Xi’an, northwestern China, *Atmos. Meas. Tech.*, 11, 3447–3456, <https://doi.org/10.5194/amt-11-3447-2018>, 2018.
- Huang, W., Saathoff, H., Shen, X., Ramisetty, R., Leisner, T., and Mohr, C.: Chemical Characterization of Highly Functionalized Organonitrates Contributing to Night-Time Organic Aerosol Mass Loadings and Particle Growth, *Environ. Sci. Technol.*, 53, 1165–1174, <https://doi.org/10.1021/acs.est.8b05826>, 2019.
- Hunter, J. F., Day, D. A., Palm, B. B., Yatavelli, R. L. N., Chan, A. W. H., Kaser, L., Cappellin, L., Hayes, P. L., Cross, E. S., Carrasquillo, A. J., Campuzano-Jost, P., Stark, H., Zhao, Y., Hohaus, T., Smith, J. N., Hansel, A., Karl, T., Goldstein, A. H., Guenther, A., Worsnop, D. R., Thornton, J. A., Heald, C. L., Jimenez, J. L., and Kroll, J. H.: Comprehensive characterization of atmospheric organic carbon at a forested site, *Nat. Geosci.*, 10, 748–753, <https://doi.org/10.1038/NGEO3018>, 2017.
- Hyttinen, N., Otkjær, R. V., Iyer, S., Kjaergaard, H. G., Rissanen, M. P., Wennberg, P. O., and Kurtén, T.: Computational Comparison of Different Reagent Ions in the Chemical Ionization of Oxidized Multifunctional Compounds, *J. Phys. Chem. A*, 122, 269–279, <https://doi.org/10.1021/acs.jpca.7b10015>, 2018.
- Isaacman-VanWertz, G., Massoli, P., O’Brien, R., Lim, C., Franklin, J., Moss, J., Hunter, J., Nowak, J., Canagaratna, M., Misztal, P., Arata, C., Roscioli, J., Herndon, S., Onasch, T., Lambe, A., Jayne, J., Su, L., Knopf, D., Goldstein, A., Worsnop, D., and Kroll, J.: Chemical evolution of atmospheric organic carbon over multiple generations of oxidation, *Nat. Chem.*, 10, 462–468, <https://doi.org/10.1038/s41557-018-0002-2>, 2018.
- Iyer, S., Lopez-Hilfiker, F., Lee, B. H., Thornton, J. A., and Kurtén, T.: Modeling the Detection of Organic and Inorganic Compounds Using Iodide-Based Chemical Ionization, *J. Phys. Chem. A*, 120, 576–587, <https://doi.org/10.1021/acs.jpca.5b09837>, 2016.
- Jacobs, M. I., Burke, W. J., and Elrod, M. J.: Kinetics of the reactions of isoprene-derived hydroxynitrates: gas phase epoxide formation and solution phase hydrolysis, *Atmos. Chem. Phys.*, 14, 8933–8946, <https://doi.org/10.5194/acp-14-8933-2014>, 2014.
- Jenkin, M. E., Saunders, S. M., Wagner, V., and Pilling, M. J.: Protocol for the development of the Master Chemical Mechanism, MCM v3 (Part B): tropospheric degradation of aromatic volatile organic compounds, *Atmos. Chem. Phys.*, 3, 181–193, <https://doi.org/10.5194/acp-3-181-2003>, 2003.
- Karl, T., Striednig, M., Graus, M., Hammerle, A., and Wohlfahrt, G.: Urban flux measurements reveal a large pool of oxygenated volatile organic compound emissions, *P. Natl. Acad. Sci. USA*, 115, 1186–1191, <https://doi.org/10.1073/pnas.1714715115>, 2018.
- Kawamura, K. and Bikkina, S.: A review of dicarboxylic acids and related compounds in atmospheric aerosols: Molecular distributions, sources and transformation, *Atmos. Res.*, 170, 140–160, <https://doi.org/10.1016/j.atmosres.2015.11.018>, 2016.
- Kawamura, K., Kasukabe, H., and Barrie, L. A.: Source and reaction pathways of dicarboxylic acids, ketoacids and dicarbonyls in arctic aerosols: One year of observations, *Atmos. Environ.*, 30, 1709–1722, [https://doi.org/10.1016/1352-2310\(95\)00395-9](https://doi.org/10.1016/1352-2310(95)00395-9), 1996.
- Kong, X., Salvador, C. M., Carlsson, S., Pathak, R., Davidsson, K. O., Le Breton, M., Gaita, S. M., Mitra, K., Hallquist, Å. M., Hallquist, M., and Pettersson, J. B. C.: Molecular characterization and optical properties of primary emissions from a residential wood burning boiler, *Sci. Total Environ.*, 754, 142143, <https://doi.org/10.1016/j.scitotenv.2020.142143>, 2021.
- Krechmer, J. E., Pagonis, D., Ziemann, P. J., and Jimenez, J. L.: Quantification of Gas-Wall Partitioning in Teflon Environmental Chambers Using Rapid Bursts of Low-Volatility Oxidized

- Species Generated in Situ, *Environ. Sci. Technol.*, 50, 5757–5765, <https://doi.org/10.1021/acs.est.6b00606>, 2016.
- Kroll, J. H. and Seinfeld, J. H.: Chemistry of secondary organic aerosol: Formation and evolution of low-volatility organics in the atmosphere, *Atmos. Environ.*, 42, 3593–3624, <https://doi.org/10.1016/j.atmosenv.2008.01.003>, 2008.
- Lambe, A. T., Onasch, T. B., Croasdale, D. R., Wright, J. P., Martin, A. T., Franklin, J. P., Massoli, P., Kroll, J. H., Canagaratna, M. R., Brune, W. H., Worsnop, D. R., and Davidovits, P.: Transitions from functionalization to fragmentation reactions of laboratory Secondary Organic Aerosol (SOA) generated from the OH oxidation of alkane precursors, *Environ. Sci. Technol.*, 46, 5430–5437, <https://doi.org/10.1021/es300274t>, 2012.
- Larsen, B. R., Di Bella, D., Glasius, M., Winterhalter, R., Jensen, N. R., and Hjorth, J.: Gas-phase OH oxidation of monoterpenes: Gaseous and particulate products, *J. Atmos. Chem.*, 38, 231–276, <https://doi.org/10.1023/A:1006487530903>, 2001.
- Le Breton, M., Hallquist, Å. M., Pathak, R. K., Simpson, D., Wang, Y., Johansson, J., Zheng, J., Yang, Y., Shang, D., Wang, H., Liu, Q., Chan, C., Wang, T., Bannan, T. J., Priestley, M., Percival, C. J., Shallcross, D. E., Lu, K., Guo, S., Hu, M., and Hallquist, M.: Chlorine oxidation of VOCs at a semi-rural site in Beijing: significant chlorine liberation from ClNO₂ and subsequent gas- and particle-phase Cl–VOC production, *Atmos. Chem. Phys.*, 18, 13013–13030, <https://doi.org/10.5194/acp-18-13013-2018>, 2018a.
- Le Breton, M., Wang, Y., Hallquist, Å. M., Pathak, R. K., Zheng, J., Yang, Y., Shang, D., Glasius, M., Bannan, T. J., Liu, Q., Chan, C. K., Percival, C. J., Zhu, W., Lou, S., Topping, D., Wang, Y., Yu, J., Lu, K., Guo, S., Hu, M., and Hallquist, M.: Online gas- and particle-phase measurements of organosulfates, organosulfonates and nitrooxy organosulfates in Beijing utilizing a FIGAERO ToF-CIMS, *Atmos. Chem. Phys.*, 18, 10355–10371, <https://doi.org/10.5194/acp-18-10355-2018>, 2018b.
- Le Breton, M., Psichoudaki, M., Hallquist, M., Watne, Å. K., Lutz, A., and Hallquist, Å. M.: Application of a FIGAERO ToF CIMS for on-line characterization of real-world fresh and aged particle emissions from buses, *Aerosol Sci. Tech.*, 53, 244–259, <https://doi.org/10.1080/02786826.2019.1566592>, 2019.
- Lee, B. H., Lopez-Hilfiker, F. D., Mohr, C., Kurtén, T., Worsnop, D. R., and Thornton, J. A.: An iodide-adduct high-resolution time-of-flight chemical-ionization mass spectrometer: Application to atmospheric inorganic and organic compounds, *Environ. Sci. Technol.*, 48, 6309–6317, <https://doi.org/10.1021/es500362a>, 2014.
- Lee, B. H., Mohr, C., Lopez-Hilfiker, F. D., Lutz, A., Hallquist, M., Lee, L., Romer, P., Cohen, R. C., Iyer, S., Kurtén, T., Hu, W., Day, D. A., Campuzano-Jost, P., Jimenez, J. L., Xu, L., Ng, N. L., Guo, H., Weber, R. J., Wild, R. J., Brown, S. S., Koss, A., de Gouw, J., Olson, K., Goldstein, A. H., Seco, R., Kim, S., McAvey, K., Shepson, P. B., Starn, T., Baumann, K., Edgerton, E. S., Liu, J., Shilling, J. E., Miller, D. O., Brune, W., Schobesberger, S., D'Ambro, E. L., and Thornton, J. A.: Highly functionalized organic nitrates in the southeast United States: Contribution to secondary organic aerosol and reactive nitrogen budgets, *P. Natl. Acad. Sci. USA*, 113, 1516–1521, <https://doi.org/10.1073/pnas.1508108113>, 2016.
- Lee, B. H., Lopez-hilfiker, F. D., Veres, P. R., McDuffie, E. E., Fibiger, D. L., Tamara, L., and Thornton, J. A.: Flight deployment of a high-resolution time-of-flight chemical ionization mass spectrometer: observations of reactive halogen and nitrogen oxide species, *J. Geophys. Res.-Atmos.*, 123, 7670–7686, <https://doi.org/10.1029/2017JD028082>, 2018a.
- Lee, B. H., Lopez-Hilfiker, F. D., D'Ambro, E. L., Zhou, P., Boy, M., Petäjä, T., Hao, L., Virtanen, A., and Thornton, J. A.: Semi-volatile and highly oxygenated gaseous and particulate organic compounds observed above a boreal forest canopy, *Atmos. Chem. Phys.*, 18, 11547–11562, <https://doi.org/10.5194/acp-18-11547-2018>, 2018b.
- Li, T., Wang, Z., Yuan, B., Ye, C., Lin, Y., Wang, S., Sha, Q., Yuan, Z., Zheng, J., and Shao, M.: Emissions of carboxylic acids, hydrogen cyanide (HCN) and isocyanic acid (HNCO) from vehicle exhaust, *Atmos. Environ.*, 247, 118218, <https://doi.org/10.1016/j.atmosenv.2021.118218>, 2021.
- Liao, J., Froyd, K. D., Murphy, D. M., Keutsch, F. N., Yu, G., Wennberg, P. O., St Clair, J. M., Crouse, J. D., Wisthaler, A., Mikoviny, T., Jimenez, J. L., Campuzano-Jost, P., Day, D. A., Hu, W., Ryerson, T. B., Pollack, I. B., Peischl, J., Anderson, B. E., Ziemba, L. D., Blake, D. R., Meinardi, S., and Diskin, G.: Airborne measurements of organosulfates over the continental U.S, *J. Geophys. Res.-Atmos.*, 120, 2990–3005, <https://doi.org/10.1002/2014JD022378>, 2015.
- Lim, H.-J., Carlton, A. G., and Turpin, B. J.: Isoprene Forms Secondary Organic Aerosol through Cloud Processing: Model Simulations, *Environ. Sci. Technol.*, 39, 4441–4446, <https://doi.org/10.1021/es048039h>, 2005.
- Liu, C., Deng, X., Zhu, B., and Yin, C.: Characteristics of GSR of China's three major economic regions in the past 10 years and its relationship with O₃ and PM_{2.5}, *China Environ. Sci.*, 38, 2820–2829, <https://doi.org/10.19674/j.cnki.issn1000-6923.2018.0295>, 2018.
- Liu, X., Qu, H., Huey, L. G., Wang, Y., Sjostedt, S., Zeng, L., Lu, K., Wu, Y., Hu, M., Shao, M., Zhu, T., and Zhang, Y.: High Levels of Daytime Molecular Chlorine and Nitryl Chloride at a Rural Site on the North China Plain, *Environ. Sci. Technol.*, 51, 9588–9595, <https://doi.org/10.1021/acs.est.7b03039>, 2017.
- Liu, Z., Wang, Y., Gu, D., Zhao, C., Huey, L. G., Stickel, R., Liao, J., Shao, M., Zhu, T., Zeng, L., Amoroso, A., Costabile, F., Chang, C.-C., and Liu, S.-C.: Summertime photochemistry during CAREBeijing-2007: RO_x budgets and O₃ formation, *Atmos. Chem. Phys.*, 12, 7737–7752, <https://doi.org/10.5194/acp-12-7737-2012>, 2012.
- Lopez-Hilfiker, F. D., Mohr, C., Ehn, M., Rubach, F., Kleist, E., Wildt, J., Mentel, Th. F., Lutz, A., Hallquist, M., Worsnop, D., and Thornton, J. A.: A novel method for online analysis of gas and particle composition: description and evaluation of a Filter Inlet for Gases and AEROSols (FIGAERO), *Atmos. Meas. Tech.*, 7, 983–1001, <https://doi.org/10.5194/amt-7-983-2014>, 2014.
- Lopez-Hilfiker, F. D., Mohr, C., Ehn, M., Rubach, F., Kleist, E., Wildt, J., Mentel, Th. F., Carrasquillo, A. J., Daumit, K. E., Hunter, J. F., Kroll, J. H., Worsnop, D. R., and Thornton, J. A.: Phase partitioning and volatility of secondary organic aerosol components formed from α -pinene ozonolysis and OH oxidation: the importance of accretion products and other low volatility compounds, *Atmos. Chem. Phys.*, 15, 7765–7776, <https://doi.org/10.5194/acp-15-7765-2015>, 2015.
- Lopez-Hilfiker, F. D., Iyer, S., Mohr, C., Lee, B. H., D'Ambro, E. L., Kurtén, T., and Thornton, J. A.: Constraining the sensitivity

- of iodide adduct chemical ionization mass spectrometry to multifunctional organic molecules using the collision limit and thermodynamic stability of iodide ion adducts, *Atmos. Meas. Tech.*, 9, 1505–1512, <https://doi.org/10.5194/amt-9-1505-2016>, 2016.
- Massoli, P., Stark, H., Canagaratna, M. R., Krechmer, J. E., Xu, L., Ng, N. L., Mauldin, R. L., Yan, C., Kimmel, J., Misztal, P. K., Jimenez, J. L., Jayne, J. T., and Worsnop, D. R.: Ambient Measurements of Highly Oxidized Gas-Phase Molecules during the Southern Oxidant and Aerosol Study (SOAS) 2013, *ACS Earth Sp. Chem.*, 2, 653–672, <https://doi.org/10.1021/acsearthspacechem.8b00028>, 2018.
- Mattila, J. M., Brophy, P., Kirkland, J., Hall, S., Ullmann, K., Fischer, E. V., Brown, S., McDuffie, E., Tevlin, A., and Farmer, D. K.: Tropospheric sources and sinks of gas-phase acids in the Colorado Front Range, *Atmos. Chem. Phys.*, 18, 12315–12327, <https://doi.org/10.5194/acp-18-12315-2018>, 2018.
- Mehra, A., Wang, Y., Krechmer, J. E., Lambe, A., Majluf, F., Morris, M. A., Priestley, M., Bannan, T. J., Bryant, D. J., Pereira, K. L., Hamilton, J. F., Rickard, A. R., Newland, M. J., Stark, H., Croteau, P., Jayne, J. T., Worsnop, D. R., Canagaratna, M. R., Wang, L., and Coe, H.: Evaluation of the chemical composition of gas- and particle-phase products of aromatic oxidation, *Atmos. Chem. Phys.*, 20, 9783–9803, <https://doi.org/10.5194/acp-20-9783-2020>, 2020.
- Mellouki, A., Wallington, T. J., and Chen, J.: Atmospheric Chemistry of Oxygenated Volatile Organic Compounds: Impacts on Air Quality and Climate, *Chem. Rev.*, 115, 3984–4014, <https://doi.org/10.1021/cr500549n>, 2015.
- Mohr, C., Lopez-Hilfiker, F. D., Zotter, P., Prévôt, A. S. H., Xu, L., Ng, N. L., Herndon, S. C., Williams, L. R., Franklin, J. P., Zahniser, M. S., Worsnop, D. R., Knighton, W. B., Aiken, A. C., Gorkowski, K. J., Dubey, M. K., Allan, J. D., and Thornton, J. A.: Contribution of Nitrated Phenols to Wood Burning Brown Carbon Light Absorption in Detling, United Kingdom during Winter Time, *Environ. Sci. Technol.*, 47, 6316–6324, <https://doi.org/10.1021/es400683v>, 2013.
- Mutzel, A., Poulain, L., Berndt, T., Iinuma, Y., Rodigast, M., Böge, O., Richters, S., Spindler, G., Sipilä, M., Jokinen, T., Kulmala, M., and Herrmann, H.: Highly Oxidized Multifunctional Organic Compounds Observed in Tropospheric Particles: A Field and Laboratory Study, *Environ. Sci. Technol.*, 49, 7754–7761, <https://doi.org/10.1021/acs.est.5b00885>, 2015.
- Mutzel, A., Rodigast, M., Iinuma, Y., Böge, O., and Herrmann, H.: Monoterpene SOA – Contribution of first-generation oxidation products to formation and chemical composition, *Atmos. Environ.*, 130, 136–144, <https://doi.org/10.1016/j.atmosenv.2015.10.080>, 2016.
- Nah, T., Sanchez, J., Boyd, C. M., and Ng, N. L.: Photochemical Aging of α -pinene and β -pinene Secondary Organic Aerosol formed from Nitrate Radical Oxidation, *Environ. Sci. Technol.*, 50, 222–231, <https://doi.org/10.1021/acs.est.5b04594>, 2016.
- Nannoolal, Y., Rarey, J., and Ramjugernath, D.: Estimation of pure component properties Part 3. Estimation of the vapor pressure of non-electrolyte organic compounds via group contributions and group interactions, *Fluid Phase Equilib.*, 269, 117–133, <https://doi.org/10.1016/j.fluid.2008.04.020>, 2008.
- Ng, N. L., Brown, S. S., Archibald, A. T., Atlas, E., Cohen, R. C., Crowley, J. N., Day, D. A., Donahue, N. M., Fry, J. L., Fuchs, H., Griffin, R. J., Guzman, M. I., Herrmann, H., Hodzic, A., Iinuma, Y., Jimenez, J. L., Kiendler-Scharr, A., Lee, B. H., Luecken, D. J., Mao, J., McLaren, R., Mutzel, A., Osthoff, H. D., Ouyang, B., Picquet-Varrault, B., Platt, U., Pye, H. O. T., Rudich, Y., Schwantes, R. H., Shiraiwa, M., Stutz, J., Thornton, J. A., Tilgner, A., Williams, B. J., and Zaveri, R. A.: Nitrate radicals and biogenic volatile organic compounds: oxidation, mechanisms, and organic aerosol, *Atmos. Chem. Phys.*, 17, 2103–2162, <https://doi.org/10.5194/acp-17-2103-2017>, 2017.
- Noelscher, A. C., Yanez-Serrano, A. M., Wolff, S., de Araujo, A. C., Lavric, J. V., Kesselmeier, J., and Williams, J.: Unexpected seasonality in quantity and composition of Amazon rainforest air reactivity, *Nat. Commun.*, 7, , 10383, <https://doi.org/10.1038/ncomms10383>, 2016.
- Osthoff, H. D., Roberts, J. M., Ravishankara, A. R., Williams, E. J., Lerner, B. M., Sommariva, R., Bates, T. S., Coffman, D., Quinn, P. K., Dibb, J. E., Stark, H., Burkholder, J. B., Talukdar, R. K., Meagher, J., Fehsenfeld, F. C., and Brown, S. S.: High levels of nitryl chloride in the polluted subtropical marine boundary layer, *Nat. Geosci.*, 1, 324–328, <https://doi.org/10.1038/ngeo177>, 2008.
- Palm, B. B., Liu, X., Jimenez, J. L., and Thornton, J. A.: Performance of a new coaxial ion–molecule reaction region for low-pressure chemical ionization mass spectrometry with reduced instrument wall interactions, *Atmos. Meas. Tech.*, 12, 5829–5844, <https://doi.org/10.5194/amt-12-5829-2019>, 2019.
- Pankow, J. F. and Asher, W. E.: SIMPOL.1: a simple group contribution method for predicting vapor pressures and enthalpies of vaporization of multifunctional organic compounds, *Atmos. Chem. Phys.*, 8, 2773–2796, <https://doi.org/10.5194/acp-8-2773-2008>, 2008.
- Paulot, F., Crouse, J. D., Kjaergaard, H. G., Kroll, J. H., Seinfeld, J. H., and Wennberg, P. O.: Isoprene photooxidation: new insights into the production of acids and organic nitrates, *Atmos. Chem. Phys.*, 9, 1479–1501, <https://doi.org/10.5194/acp-9-1479-2009>, 2009.
- Qi, L., Chen, M., Stefenelli, G., Pospisilova, V., Tong, Y., Bertrand, A., Hueglin, C., Ge, X., Baltensperger, U., Prévôt, A. S. H., and Slowik, J. G.: Organic aerosol source apportionment in Zurich using an extractive electrospray ionization time-of-flight mass spectrometer (EESI-TOF-MS) – Part 2: Biomass burning influences in winter, *Atmos. Chem. Phys.*, 19, 8037–8062, <https://doi.org/10.5194/acp-19-8037-2019>, 2019.
- Reyes-Villegas, E., Bannan, T., Le Breton, M., Mehra, A., Priestley, M., Percival, C., Coe, H., and Allan, J. D.: Online Chemical Characterization of Food-Cooking Organic Aerosols: Implications for Source Apportionment, *Environ. Sci. Technol.*, 52, 5308–5318, <https://doi.org/10.1021/acs.est.7b06278>, 2018.
- Riva, M., Rantala, P., Krechmer, J. E., Peräkylä, O., Zhang, Y., Heikkinen, L., Garmash, O., Yan, C., Kulmala, M., Worsnop, D., and Ehn, M.: Evaluating the performance of five different chemical ionization techniques for detecting gaseous oxygenated organic species, *Atmos. Meas. Tech.*, 12, 2403–2421, <https://doi.org/10.5194/amt-12-2403-2019>, 2019.
- Sander, R. and Crutzen, P. J.: Model study indicating halogen activation and ozone destruction in polluted air masses transported to the sea, *J. Geophys. Res.-Atmos.*, 101, 9121–9138, <https://doi.org/10.1029/95JD03793>, 1996.
- Schneider, J., Weimer, S., Drewnick, F., Borrmann, S., Helas, G., Gwaze, P., Schmid, O., Andreae, M. O., and Kirchner, U.: Mass

- spectrometric analysis and aerodynamic properties of various types of combustion-related aerosol particles, *Int. J. Mass Spectrom.*, 258, 37–49, <https://doi.org/10.1016/j.ijms.2006.07.008>, 2006.
- Schwantes, R. H., Teng, A. P., Nguyen, T. B., Coggon, M. M., Crouse, J. D., St Clair, J. M., Zhang, X., Schilling, K. A., Seinfeld, J. H., and Wennberg, P. O.: Isoprene NO₃ Oxidation Products from the RO₂ + HO₂ Pathway, *J. Phys. Chem. A*, 119, 10158, <https://doi.org/10.1021/acs.jpca.5b06355>, 2015.
- Schwantes, R. H., Schilling, K. A., McVay, R. C., Lignell, H., Coggon, M. M., Zhang, X., Wennberg, P. O., and Seinfeld, J. H.: Formation of highly oxygenated low-volatility products from cresol oxidation, *Atmos. Chem. Phys.*, 17, 3453–3474, <https://doi.org/10.5194/acp-17-3453-2017>, 2017.
- Schwantes, R. H., Emmons, L. K., Orlando, J. J., Barth, M. C., Tyn-dall, G. S., Hall, S. R., Ullmann, K., St. Clair, J. M., Blake, D. R., Wisthaler, A., and Bui, T. P. V.: Comprehensive isoprene and terpene gas-phase chemistry improves simulated surface ozone in the southeastern US, *Atmos. Chem. Phys.*, 20, 3739–3776, <https://doi.org/10.5194/acp-20-3739-2020>, 2020.
- Shrivastava, M., Andreae, M. O., Artaxo, P., Barbosa, H. M. J., Berg, L. K., Brito, J., Ching, J., Easter, R. C., Fan, J., Fast, J. D., Feng, Z., Fuentes, J. D., Glasius, M., Goldstein, A. H., Alves, E. G., Gomes, H., Gu, D., Guenther, A., Jathar, S. H., Kim, S., Liu, Y., Lou, S., Martin, S. T., McNeill, V. F., Medeiros, A., de Sá, S. S., Shilling, J. E., Springston, S. R., Souza, R. A. F., Thornton, J. A., Isaacman-VanWertz, G., Yee, L. D., Ynoue, R., Zaveri, R. A., Zelenyuk, A., and Zhao, C.: Urban pollution greatly enhances formation of natural aerosols over the Amazon rainforest, *Nat. Commun.*, 10, 1046, <https://doi.org/10.1038/s41467-019-08909-4>, 2019.
- Simoneit, B. R. T., Schauer, J. J., Nolte, C. G., Oros, D. R., Elias, V. O., Fraser, M. P., Rogge, W. F., and Cass, G. R.: Levoglucosan, a tracer for cellulose in biomass burning and atmospheric particles, *Atmos. Environ.*, 33, 173–182, [https://doi.org/10.1016/S1352-2310\(98\)00145-9](https://doi.org/10.1016/S1352-2310(98)00145-9), 1999.
- Slusher, D. L., Huey, L. G., Tanner, D. J., Flocke, F. M., and Roberts, J. M.: A thermal dissociation–chemical ionization mass spectrometry (TD-CIMS) technique for the simultaneous measurement of peroxyacyl nitrates and dinitrogen pentoxide, *J. Geophys. Res.-Atmos.*, 109, D19315, <https://doi.org/10.1029/2004JD004670>, 2004.
- Stark, H., Yatavelli, R. L. N., Thompson, S. L., Kimmel, J. R., Cubison, M. J., Chhabra, P. S., Canagaratna, M. R., Jayne, J. T., Worsnop, D. R., and Jimenez, J. L.: Methods to extract molecular and bulk chemical information from series of complex mass spectra with limited mass resolution, *Int. J. Mass Spectrom.*, 389, 26–38, <https://doi.org/10.1016/j.ijms.2015.08.011>, 2015.
- Stark, H., Yatavelli, R. L. N., Thompson, S. L., Kang, H., Krechmer, J. E., Kimmel, J. R., Palm, B. B., Hu, W., Hayes, P. L., Day, D. A., Campuzano-Jost, P., Canagaratna, M. R., Jayne, J. T., Worsnop, D. R., and Jimenez, J. L.: Impact of Thermal Decomposition on Thermal Desorption Instruments: Advantage of Thermogram Analysis for Quantifying Volatility Distributions of Organic Species, *Environ. Sci. Technol.*, 51, 8491–8500, <https://doi.org/10.1021/acs.est.7b00160>, 2017.
- Stolzenburg, D., Fischer, L., Vogel, A. L., Heinritzi, M., Schervish, M., Simon, M., Wagner, A. C., Dada, L., Ahonen, L. R., Amorim, A., Baccarini, A., Bauer, P. S., Baumgartner, B., Bergen, A., Bianchi, F., Breitenlechner, M., Brilke, S., Buenrostro Mazon, S., Chen, D., Dias, A., Draper, D. C., Duplissy, J., El Haddad, I., Finkenzeller, H., Frege, C., Fuchs, C., Garmash, O., Gordon, H., He, X., Helm, J., Hofbauer, V., Hoyle, C. R., Kim, C., Kirkby, J., Kontkanen, J., Kürten, A., Lampilahti, J., Lawler, M., Lehtipalo, K., Leiminger, M., Mai, H., Mathot, S., Mentler, B., Molteni, U., Nie, W., Nieminen, T., Nowak, J. B., Ojdanic, A., Onnela, A., Passananti, M., Petäjä, T., Quéléver, L. L. J., Rissanen, M. P., Sarnela, N., Schallhart, S., Tauber, C., Tomé, A., Wagner, R., Wang, M., Weitz, L., Wimmer, D., Xiao, M., Yan, C., Ye, P., Zha, Q., Baltensperger, U., Curtius, J., Dommen, J., Flagan, R. C., Kulmala, M., Smith, J. N., Worsnop, D. R., Hansel, A., Donahue, N. M., Winkler, P. M., Nie, W., Passananti, M., Leiminger, M., Stolzenburg, D., Yan, C., Wimmer, D., Buenrostro Mazon, S., Kontkanen, J., Wang, M., Garmash, O., Kulmala, M., Petäjä, T., Bianchi, F., Chen, D., Nieminen, T., Brilke, S., Nowak, J. B., Duplissy, J., El Haddad, I., Simon, M., Wagner, A. C., Kürten, A., Smith, J. N., Kim, C., et al.: Rapid growth of organic aerosol nanoparticles over a wide tropospheric temperature range, *P. Natl. Acad. Sci.*, 115, 201807604, <https://doi.org/10.1073/pnas.1807604115>, 2018.
- Surratt, J. D., Murphy, S. M., Kroll, J. H., Ng, N. L., Hildebrandt, L., Sorooshian, A., Szmigielski, R., Vermeylen, R., Maenhaut, W., Claeys, M., Flagan, R. C., and Seinfeld, J. H.: Chemical Composition of Secondary Organic Aerosol Formed from the Photooxidation of Isoprene, *J. Phys. Chem. A*, 110, 9665–9690, <https://doi.org/10.1021/jp061734m>, 2006.
- Surratt, J. D., Kroll, J. H., Kleindienst, T. E., Edney, E. O., Claeys, M., Sorooshian, A., Ng, N. L., Offenberg, J. H., Lewandowski, M., Jaoui, M., Flagan, R. C., and Seinfeld, J. H.: Evidence for Organosulfates in Secondary Organic Aerosol, *Environ. Sci. Technol.*, 41, 517–527, <https://doi.org/10.1021/es062081q>, 2007.
- Surratt, J. D., Chan, A. W. H., Eddingsaas, N. C., Chan, M., Loza, C. L., Kwan, A. J., Hersey, S. P., Flagan, R. C., Wennberg, P. O., and Seinfeld, J. H.: Reactive intermediates revealed in secondary organic aerosol formation from isoprene, *P. Natl. Acad. Sci. USA*, 107, 6640–6645, <https://doi.org/10.1073/pnas.0911114107>, 2010.
- Thornton, J. A., Mohr, C., Schobesberger, S., D’Ambro, E. L., Lee, B. H., and Lopez-Hilfiker, F. D.: Evaluating Organic Aerosol Sources and Evolution with a Combined Molecular Composition and Volatility Framework Using the Filter Inlet for Gases and Aerosols (FIGAERO), *Acc. Chem. Res.*, 53, 1415–1426, <https://doi.org/10.1021/acs.accounts.0c00259>, 2020.
- Volkamer, R., Jimenez, J. L., San Martini, F., Dzepina, K., Zhang, Q., Salcedo, D., Molina, L. T., Worsnop, D. R., and Molina, M. J.: Secondary organic aerosol formation from anthropogenic air pollution: Rapid and higher than expected, *Geophys. Res. Lett.*, 33, L17811, <https://doi.org/10.1029/2006GL026899>, 2006.
- Wang, H., Gao, Y., Wang, S., Wu, X., Liu, Y., Li, X., Huang, D., Lou, S., Wu, Z., Guo, S., Jing, S., Li, Y., Huang, C., Tyn-dall, G. S., Orlando, J. J., and Zhang, X.: Atmospheric Processing of Nitrophenols and Nitrocresols from Biomass Burning Emissions, *J. Geophys. Res.-Atmos.*, 125, e2020JD033401, <https://doi.org/10.1029/2020JD033401>, 2020.
- Wang, M., Chen, D., Xiao, M., Ye, Q., Stolzenburg, D., Hofbauer, V., Ye, P., Vogel, A. L., Mauldin, R. L., Amorim, A., Baccarini, A., Baumgartner, B., Brilke, S., Dada, L., Dias, A., Duplissy, J., Finkenzeller, H., Garmash, O., He, X.-C., Hoyle, C. R., Kim,

- C., Kvashnin, A., Lehtipalo, K., Fischer, L., Molteni, U., Petäjä, T., Pospisilova, V., Quéléver, L. L. J., Rissanen, M., Simon, M., Tauber, C., Tomé, A., Wagner, A. C., Weitz, L., Volkamer, R., Winkler, P. M., Kirkby, J., Worsnop, D. R., Kulmala, M., Baltensperger, U., Dommen, J., El-Haddad, I., and Donahue, N. M.: Photo-oxidation of Aromatic Hydrocarbons Produces Low-Volatility Organic Compounds, *Environ. Sci. Technol.*, 54, 7911–7921, <https://doi.org/10.1021/acs.est.0c02100>, 2020.
- Wang, Q., He, X., Zhou, M., Huang, D. D., Qiao, L., Zhu, S., Ma, Y., Wang, H., Li, L., Huang, C., Huang, X. H. H., Xu, W., Worsnop, D., Goldstein, A. H., Guo, H., and Yu, J. Z.: Hourly Measurements of Organic Molecular Markers in Urban Shanghai, China: Primary Organic Aerosol Source Identification and Observation of Cooking Aerosol Aging, *ACS Earth Sp. Chem.*, 4, 1670–1685, <https://doi.org/10.1021/acsearthspacechem.0c00205>, 2020.
- Wang, T., Tham, Y. J., Xue, L., Li, Q., Zha, Q., Wang, Z., Poon, S. C. N., Dube, W. P., Blake, D. R., Louie, P. K. K., Luk, C. W. Y., Tsui, W., Brown, S. S., Osthoff, H. D., Roberts, J. M., Ravishankara, A. R., Williams, E. J., Lerner, B. M., Sommariva, R., Bates, T. S., Coffman, D., Quinn, P. K., Dibb, J. E., Stark, H., Burkholder, J. B., Talukdar, R. K., Meagher, J., Fehsenfeld, F. C., and Brown, S. S.: Observations of nitryl chloride and modeling its source and effect on ozone in the planetary boundary layer of southern China, *J. Geophys. Res.*, 121, 2476–2489, <https://doi.org/10.1002/2015JD024556>, 2016.
- Wang, X., Jacob, D. J., Eastham, S. D., Sulprizio, M. P., Zhu, L., Chen, Q., Alexander, B., Sherwen, T., Evans, M. J., Lee, B. H., Haskins, J. D., Lopez-Hilfiker, F. D., Thornton, J. A., Huey, G. L., and Liao, H.: The role of chlorine in global tropospheric chemistry, *Atmos. Chem. Phys.*, 19, 3981–4003, <https://doi.org/10.5194/acp-19-3981-2019>, 2019.
- Wang, Z., Yuan, B., Ye, C., Roberts, J., Wisthaler, A., Lin, Y., Li, T., Wu, C., Peng, Y., Wang, C., Wang, S., Yang, S., Wang, B., Qi, J., Wang, C., Song, W., Hu, W., Wang, X., Xu, W., Ma, N., Kuang, Y., Tao, J., Zhang, Z., Su, H., Cheng, Y., Wang, X., and Shao, M.: High Concentrations of Atmospheric Isocyanic Acid (HNCO) Produced from Secondary Sources in China, *Environ. Sci. Technol.*, 11818–11826, <https://doi.org/10.1021/acs.est.0c02843>, 2020.
- Wennberg, P. O., Bates, K. H., Crounse, J. D., Dodson, L. G., McVay, R. C., Mertens, L. A., Nguyen, T. B., Praske, E., Schwantes, R. H., Smarte, M. D., St Clair, J. M., Teng, A. P., Zhang, X., and Seinfeld, J. H.: Gas-Phase Reactions of Isoprene and Its Major Oxidation Products, *Chem. Rev.*, 118, 3337–3390, <https://doi.org/10.1021/acs.chemrev.7b00439>, 2018.
- Wu, C., Wang, C., Wang, S., Wang, W., Yuan, B., Qi, J., Wang, B., Wang, H., Wang, C., Song, W., Wang, X., Hu, W., Lou, S., Ye, C., Peng, Y., Wang, Z., Huangfu, Y., Xie, Y., Zhu, M., Zheng, J., Wang, X., Jiang, B., Zhang, Z., and Shao, M.: Measurement report: Important contributions of oxygenated compounds to emissions and chemistry of volatile organic compounds in urban air, *Atmos. Chem. Phys.*, 20, 14769–14785, <https://doi.org/10.5194/acp-20-14769-2020>, 2020.
- Xiong, F., McAvey, K. M., Pratt, K. A., Groff, C. J., Hostetler, M. A., Lipton, M. A., Starn, T. K., Seeley, J. V., Bertman, S. B., Teng, A. P., Crounse, J. D., Nguyen, T. B., Wennberg, P. O., Mistral, P. K., Goldstein, A. H., Guenther, A. B., Koss, A. R., Olson, K. F., de Gouw, J. A., Baumann, K., Edgerton, E. S., Feiner, P. A., Zhang, L., Miller, D. O., Brune, W. H., and Shepson, P. B.: Observation of isoprene hydroxynitrates in the southeastern United States and implications for the fate of NO_x, *Atmos. Chem. Phys.*, 15, 11257–11272, <https://doi.org/10.5194/acp-15-11257-2015>, 2015.
- Xue, L., Gu, R., Wang, T., Wang, X., Saunders, S., Blake, D., Louie, P. K. K., Luk, C. W. Y., Simpson, I., Xu, Z., Wang, Z., Gao, Y., Lee, S., Mellouki, A., and Wang, W.: Oxidative capacity and radical chemistry in the polluted atmosphere of Hong Kong and Pearl River Delta region: analysis of a severe photochemical smog episode, *Atmos. Chem. Phys.*, 16, 9891–9903, <https://doi.org/10.5194/acp-16-9891-2016>, 2016.
- Yang, Y., Shao, M., Wang, X., Nölscher, A. C., Kessel, S., Guenther, A., and Williams, J.: Towards a quantitative understanding of total OH reactivity: A review, *Atmos. Environ.*, 134, 147–161, <https://doi.org/10.1016/j.atmosenv.2016.03.010>, 2016.
- Yang, Y., Shao, M., Keßel, S., Li, Y., Lu, K., Lu, S., Williams, J., Zhang, Y., Zeng, L., Nölscher, A. C., Wu, Y., Wang, X., and Zheng, J.: How the OH reactivity affects the ozone production efficiency: case studies in Beijing and Heshan, China, *Atmos. Chem. Phys.*, 17, 7127–7142, <https://doi.org/10.5194/acp-17-7127-2017>, 2017.
- Yasmeen, F., Szmigielski, R., Vermeylen, R., Gomez-Gonzalez, Y., Surratt, J. D., Chan, A. W. H., Seinfeld, J. H., Maenhaut, W., and Claeys, M.: Mass spectrometric characterization of isomeric terpenic acids from the oxidation of α -pinene, β -pinene, *d*-limonene, and Δ^3 -carene in fine forest aerosol, *J. Mass Spectrom.*, 46, 425–442, <https://doi.org/10.1002/jms.1911>, 2011.
- Yatavelli, R. L. N., Lopez-Hilfiker, F., Wargo, J. D., Kimmel, J. R., Cubison, M. J., Bertram, T. H., Jimenez, J. L., Gonin, M., Worsnop, D. R., and Thornton, J. A.: A Chemical Ionization High-Resolution Time-of-Flight Mass Spectrometer Coupled to a Micro Orifice Volatilization Impactor (MOVI-HRToF-CIMS) for Analysis of Gas and Particle-Phase Organic Species, *Aerosol Sci. Tech.*, 46, 1313–1327, <https://doi.org/10.1080/02786826.2012.712236>, 2012.
- Yuan, B., Veres, P. R., Warneke, C., Roberts, J. M., Gilman, J. B., Koss, A., Edwards, P. M., Graus, M., Kuster, W. C., Li, S.-M., Wild, R. J., Brown, S. S., Dubé, W. P., Lerner, B. M., Williams, E. J., Johnson, J. E., Quinn, P. K., Bates, T. S., Lefer, B., Hayes, P. L., Jimenez, J. L., Weber, R. J., Zamora, R., Ervens, B., Millet, D. B., Rappenglück, B., and de Gouw, J. A.: Investigation of secondary formation of formic acid: urban environment vs. oil and gas producing region, *Atmos. Chem. Phys.*, 15, 1975–1993, <https://doi.org/10.5194/acp-15-1975-2015>, 2015.
- Yuan, B., Liggio, J., Wentzell, J., Li, S.-M., Stark, H., Roberts, J. M., Gilman, J., Lerner, B., Warneke, C., Li, R., Leithead, A., Osthoff, H. D., Wild, R., Brown, S. S., and de Gouw, J. A.: Secondary formation of nitrated phenols: insights from observations during the Uintah Basin Winter Ozone Study (UBWOS) 2014, *Atmos. Chem. Phys.*, 16, 2139–2153, <https://doi.org/10.5194/acp-16-2139-2016>, 2016.
- Yuan, B., Koss, A. R., Warneke, C., Coggon, M., Sekimoto, K., and De Gouw, J. A.: Proton-Transfer-Reaction Mass Spectrometry: Applications in Atmospheric Sciences, *Chem. Rev.*, 117, 13187–13229, <https://doi.org/10.1021/acs.chemrev.7b00325>, 2017.
- Zhang, Q., Yuan, B., Shao, M., Wang, X., Lu, S., Lu, K., Wang, M., Chen, L., Chang, C.-C., and Liu, S. C.: Variations of ground-level O₃ and its precursors in Beijing in summertime

- between 2005 and 2011, *Atmos. Chem. Phys.*, 14, 6089–6101, <https://doi.org/10.5194/acp-14-6089-2014>, 2014.
- Zhang, Y. J., Tang, L. L., Wang, Z., Yu, H. X., Sun, Y. L., Liu, D., Qin, W., Canonaco, F., Prévôt, A. S. H., Zhang, H. L., and Zhou, H. C.: Insights into characteristics, sources, and evolution of submicron aerosols during harvest seasons in the Yangtze River delta region, China, *Atmos. Chem. Phys.*, 15, 1331–1349, <https://doi.org/10.5194/acp-15-1331-2015>, 2015.
- Zhao, R.: The Recent Development and Application of Chemical Ionization Mass Spectrometry in Atmospheric Chemistry, in: *Encyclopedia of Analytical Chemistry*, American Cancer Society, John Wiley & Sons, Ltd., Chichester, UK, 1–33, 2018.
- Zhao, Y., Nguyen, N. T., Presto, A. A., Hennigan, C. J., May, A. A., and Robinson, A. L.: Intermediate Volatility Organic Compound Emissions from On-Road Gasoline Vehicles and Small Off-Road Gasoline Engines, *Environ. Sci. Technol.*, 50, 4554–4563, <https://doi.org/10.1021/acs.est.5b06247>, 2016.
- Zhou, Y., Huang, X. H., Bian, Q., Griffith, S. M., Louie, P. K. K., and Yu, J. Z.: Sources and atmospheric processes impacting oxalate at a suburban coastal site in Hong Kong: Insights inferred from 1 year hourly measurements, *J. Geophys. Res.-Atmos.*, 120, 9772–9788, <https://doi.org/10.1002/2015JD023531>, 2015.